Netherlands Institute for Space Research

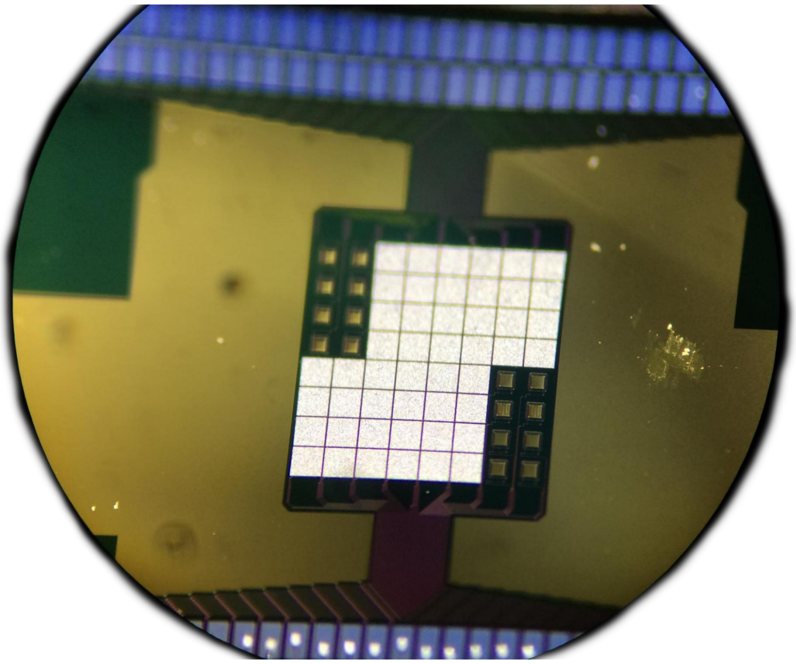

Speeding up the optimization process for Transition Edge Sensors

Finding correlations between X-ray energy resolution and Transition Edge Sensor characteristics

BSc Graduation Internship Thesis in Programme Applied Physics

Gerwin Verkerk

THE HAGUE UNIVERSITY OF APPLIED SCIENCES

SRON - Instrument Science Group
NETHERLANDS INSTITUTE FOR SPACE RESEARCH
Utrecht, Netherlands 2019 2019

Applied Physics Graduation Thesis 2019

Speeding up the optimization process for Transition Edge Sensors

Finding correlations between X-ray energy resolution and Transition Edge Sensor characteristics

Gerwin Verkerk

Faculty of Technology, Innovation & Society
Applied Physics

The Hague University of Applied Sciences
Delft, The Netherlands 2019

In this thesis, correlations between the X-ray energy resolution of TES microcalorimeters and TES characteristics are derived.

Gerwin Verkerk, 2019.

Supervisor: Dr. H. Akamatsu, SRON
Examiner: J.H.R. Lambers, The Hague University of Applied Sciences

Graduation Thesis 2019
Faculty of Technology, Innovation & Society
Applied Physics
The Hague University of Applied Sciences
Rotterdamseweg 137, 2628 AL Delft
Telephone +31 15 260 6200

Gerwin Verkerk
SRON - Instrument Science Group
Netherlands Institute for Space Research
Utrecht, Netherlands 2019

Abstract

SRON is the Dutch national expertise institute for scientific space research and is part of NWO. It plays an important role in delivering contributions to the national and international space-research communities. Currently one of SRON's involvements is in the X-IFU instrument for the Athena space X-ray observatory.

The X-IFU instrument on Athena consists of a molybdenum-gold Transition Edge Sensor (TES) array at its heart. These TES-detectors make use of the sharp superconducting transition and have a high sensitivity to small temperature changes. Each of the TES microcalorimeters in the array is referred to as a pixel. Each of the pixels is cooled to sub kelvin levels and readout under Frequency Domain Multiplexing (FDM).

The pixels have to deliver a high spectral energy resolution of 2.5 eV up to energies of 7.0 keV. To do this, the pixels are biased at specific frequencies and voltages to work under FDM and to select a point in their super to normal transition.

To verify the X-ray energy resolution of a TES microcalorimeter, a lengthy measurement has to be taken which can take over an hour for each time a parameter value is changed. Finding the optimum parameter values for one pixel can take up to a full day. For this reason, methods in quickly identifying the best values for the parameters without the need of taking long X-ray resolution measurements are searched for.

One method tested in this thesis is to look at the characteristic IV-curve of the TES-sensor, together with a phase curve that shows oscillations present in the superconducting transition. A circuit scan can also be made which shows important properties of the components connected to the TES, such as the LC-resonator resonance frequency. Statistics regarding the X-ray energy resolution dependency on different values of the tuning parameters were searched for in this thesis. Measurements of the X-ray energy resolutions dependency on the AC-bias frequency, voltage and slope in the superconducting transition were performed.

The correlation between the X-ray energy resolution and the AC-bias frequency showed that the best X-ray energy resolutions are achieved right at or close to the LC-resonator resonance frequency. The correlation was not able to be described by a fit since the scatter in the obtained measurements is too large. If this scatter is caused by a systematic error then it could be removed by repeating the measurements several times and averaging the results.

When the bias voltage across the TES is changed, the X-ray energy resolution of the TES becomes more sensitive to the AC-bias frequency. This is because a lower voltage brings the TES at a lower point in its transition and gives it a lower resistance. This causes the Q-factor of the circuit to increase and sharpens the peak at the resonance frequency of the LC-resonator.

The slope in the phase curve of the TES seems to be unimportant in determining the X-ray energy resolution. It was tested for a TES which works at a relatively low AC-bias frequency. For pixels working at higher frequencies, the effect could become of bigger importance as the oscillation caused by the weak link effect becomes larger.

Keywords: TES, microcalorimeter, X-ray, energy, resolution, X-IFU, Athena, characteristics, dependency, correlation.

Acknowledgements

I am grateful for the opportunity I've had to be a part of the Instrument Science Group at SRON. I would like to thank my supervisor Hiroki Akamatsu for his support and guidance in the work that I have done. I have learned a lot of useful things from him which I will be able to also use in other fields. I was amazed by his knowledge and ability to explain to me the immensely complex measurement setup I have worked with. This is quite a challenge for the very tight time window of the graduation internship.

Besides my supervisor, I would like to thank Luciano Gottardi and Kevin Ravensberg for their involvement in my project. They have helped me to understand the system and supplied me with constant feedback on my results. Besides that, they also came with a lot of suggestions which I greatly appreciated.

Gerwin Verkerk, Utrecht, May 2019

Contents

1
Introduction

1.1 SRON and the Instrument Science Group

SRON is the Dutch national expertise institute for scientific space research and is part of NWO. The institute was founded in the early 1960s by university groups and today offers key contributions to instruments for missions of major space agencies such as ESA, NASA and JAXA.

The contributions delivered by SRON have enabled the national and international space-research communities to explore the Universe and to investigate the Earth's atmosphere and climate. SRON also visions to continue belonging to the international forefront in the search for answers of the most fundamental existential and societal questions of mankind: What is the origin of the universe and what is it made of? Is there life elsewhere in the universe? What is the future of the Earth's climate? What are the atmospheric processes that govern changes in the Earth's climate and air quality? What role does human activity play? [1]

This graduation internship took place at SRON's instrument science group. The instrument science group develops novel detectors and detection techniques for space and Earth research instrumentation. It also validates and calibrates the instruments, on the ground and in space. Currently, a lot of focus is on the development, calibration and operation of spectrometers for gas atmospheric missions such as ESA's Sentinel-5, and its precursor TROPOMI. For the Astrophysics programme, management, system engineering, and X-ray instrumentation is applied to the Soft X-ray Spectrometers (SXS) of JAXA's Astro-H mission and the X-ray Integral Field Unit (X-IFU) of ESA's Athena mission. [2]

1.2 X-IFU on Athena

The X-IFU is the cryogenic micro-calorimeter of the Athena space X-ray observatory, the second large mission of the Cosmic Vision Program of the European Space Agency. It is designed to 1: study the dynamical physical and chemical properties of hot plasmas, such as those found in clusters of galaxies, and 2: study black hole accretion disks, jets, outflows and winds from galactic stellar mass black holes to the supermassive ones found in active galactic nuclei. [3]

To perform these researches, the instrument will have a molybdenum-gold Transition Edge Sensor (TES) array at its heart. This array will consist of 3840 individual TES's all cooled to a sub kelvin level of about 90 mK, with the bath temperature at about 50 mK [3]. It is at these low temperatures that the sensors are most sensitive in their superconducting transition.

The instrument has certain performance requirements to be able to collect the required data. The requirements set for the instrument are that it has to work in the energy range of 0.2-12.0 keV and also has to have a spectral energy resolution of 2.5 eV, up to an energy of 7.0 keV. The key performance requirements are given in table 1.1.

Table 1.1: `X-IFU key performance requirements. [3]`

Energy range	0.2–12.0 keV
Spectral resolution	2.5 eV (up to 7.0 keV)
Non X-ray background	5×10^{-3} counts/s/cm^2/keV (2-10 keV)
2.5 eV throughput (broadband, point source)	80% at 1 mCrab (10 mCrab as a goal)
10 eV throughput (5-8 keV, point source)	50% at 1 Crab
2.5 eV throughput (broadband, extended source)	80% at 2×10^{-11} ergs/s/cm^2/arcmin^2 (0.2-12 keV)
Continuous cool time	32 hours

The key technology to readout the TES sensor array will be Frequency Domain Multiplexing. This enables to read 40 TES simultaneously in one single channel and thereby makes it possible for the whole TES array to be read out by only 96 readout channels. [3]

1.3 Internship Assignment

The goal of the internship is to derive statistics regarding the X-ray energy resolution dependency on different values for the tuning parameters and TES characteristics. From these statistics, an indication for which values to pick, to achieve a high X-ray energy resolution, should be extracted.

The internship assignment focusses on an array of TES microcalorimeters similar to the ones that will be used in the X-IFU instrument for the Athena mission. These sensors are very sensitive and are able to determine the energy of incoming photons with high accuracy and resolution.

The resolution of a TES depends on certain tuning parameters such as the AC-bias frequency, AC-bias voltage, temperature and magnetic field. Determining the optimum values for these parameters is done by taking gross guesses based on measurement experience. There is not yet a statistically proven method in order to do this.

Determining the optimum point without a statistical guideline takes a lot of time. After a parameter value is changed, an X-ray resolution measurement has to be done to verify the energy resolution. These measurements can take up to an hour every time a parameter value is changed. To optimize one pixel can take up to a full day. For the 3840 pixels on the X-IFU instrument, this would too long.

There are other measurements which can be taken in a matter of minutes. These are measurements in which an characteristic IV-curve of the TES-sensor is made. This IV-curve shows the current that flows through the TES for different bias voltages and can be done for different bias frequencies. This IV-curve shows the superconducting transition of the TES-sensor and oscillations present in this transition. The task here is to derive correlations between the measurements that can be taken fast, such as the IV-curve measurement, and the X-ray energy resolution.

2

Theory

2.1 X-ray spectroscopy

X-ray radiation is a form of electromagnetic radiation with a photon energy between approximately 0.1 and 100 keV. It is caused by different generation mechanics such as the transition of electrons to lower energy levels in atoms, black body radiation, bremsstrahlung, cyclotron radiation, synchrotron radiation and inverse Compton scattering [4].

The shape of the continuous radiation spectra is determined by the conditions at which the radiation was produced. When the radiation is produced by the transition of electrons to lower energy levels in atoms, there will be certain characteristic emission lines in the spectrum. This is caused by ionisation of an element by highly energetic photons. These photons can knock out electrons in the K-shell of an atom which leaves a gap. This gap is quickly filled up by electrons from higher energy shells (L and M), releasing the excess energy as X-ray radiation [5].

It is also possible for radiation to be absorbed when it passes through a certain element. This will cause absorption lines instead of emission lines, also characteristic for the element involved.

All materials with an atomic number higher than 5 [5] can be identified using these techniques.

The characteristic X-ray spectrum for molybdenum is illustrated in figure 2.1. As can be seen from the figure, two sharp peaks exist. These peaks lay at wavelengths corresponding to the energy released when an electron falls from the L-shell or M-shell to the K-shell (Kα and Kβ). Similar spectra with characteristic peaks at other locations exist for different materials.

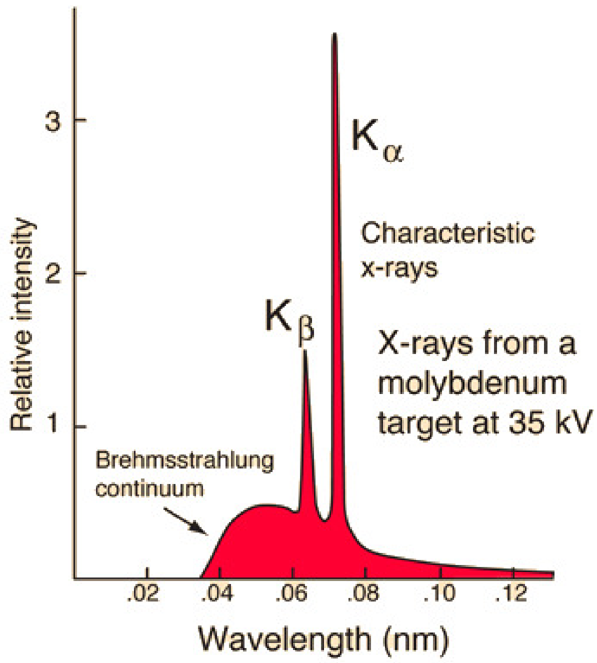

Figure 2.1: Illustration of the spectrum that would be obtained when measuring the characteristic x-rays of molybdenum. [6]

X-ray emission can be measured using an X-ray spectrometer. There exists a variety of different spectrometers with different techniques used in measuring X-ray photons. The spectrometer used in this thesis is a TES microcalorimeter. This spectrometer is based on the superconducting transition in materials. Details on how this detector works and reacts to radiation are found in the sections below.

2.2 Superconductivity

Superconductivity was first discovered in 1911, while studying the properties of matter at very low temperatures. It was discovered that the electrical resistance of mercury abruptly drops to zero when it is cooled below its critical temperature T_c of 4.2 K. This was the very first observation of superconductivity. After that discovery, it was found that the majority of chemical elements become superconducting at sufficiently low temperatures [7]. An example of this transition can be seen in figure 2.2. In this figure, the transition of a superconducting film from the normal to the superconducting state near 96 mK is shown.

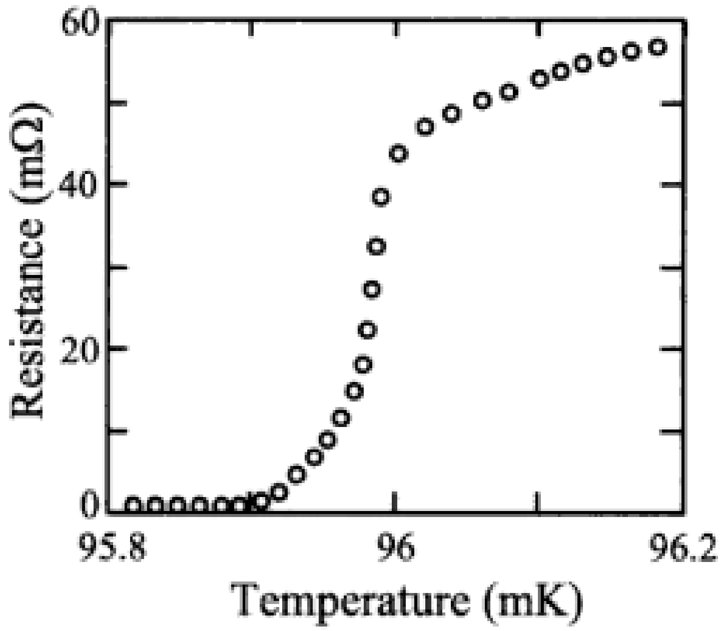

Figure 2.2: Superconducting phase transition of a superconducting film (a Mo/Cu proximity bilayer). Near 96 mK the material goes from its normal state to its superconducting state. Due to the sharp phase transition useage in sensitive thermometers is possible. [8]

Superconductivity is based on attractive electron-electron interactions which lead to the formation of Cooper pairs [4]. The electrons in Cooper pairs, behave very differently from single electrons. Single electrons are fermions (particles with half-integer spin i.e. electrons, protons and neutrons [9]) and therefore are constrained by the Pauli exclusion principle. Pairs of electrons on the other hand act more like bosons which are allowed to condense into the same energy level. Electron pairs leave an energy gap on the order of 0,001 eV that inhibits the kind of collisions that lead to a material having resistance. When the temperature is so low that the thermal energy is less than the energy of this energy gap, the material exhibits zero resistivity. [10]

When a material is in its superconducting state, it gains two important properties. These properties are the disappearance of electrical resistivity and the exclusion of magnetic fields from the superconducting material. These phenomena are described respectively by the Bardeen–Cooper–Schrieffer theory (BCS theory) and the Meissner effect. [11]

It is possible to remove the superconducting effect by applying a magnetic field stronger than the critical field H_c. The value of this critical field is temperature and material dependent. It can also be removed by applying a current larger than the critical current I_c, because a current will also induce a magnetic field. [4]

There exist two types of superconductors: type I and type II. A type I superconductor is generally made from a single element while a type II is made out of alloys. A detailed explanation of both types is given by the BCS theory. [4]

2.3 Transition-Edge Sensor (TES)

A transition-edge sensor, also mentioned as TES, is a cryogenic thermistor which is based on the sharp superconducting transition in materials. Because the phase transition of a superconducting material is so sharp, with respect to the temperature, it possible to use it as an extremely sensitive thermometer.

A TES can be used in either one of two ways; as a bolometer and as a calorimeter. When used as a bolometer its purpose is to measure a constant flow of power, and when used as a calorimeter it can detect energy pulses, such as X-ray photons.

The TES-microcalorimeter is able to achieve high energy resolutions because the response to small temperature changes is high. Small changes in temperature cause big changes in resistance. Because of this, the energy of incoming photons can be derived with high accuracy. [8]

A conventional TES-bolometer or TES-(micro)calorimeter works by having an absorber which is connected to a heat bath with a certain temperature of T_0. The coupling to the bath has a thermal conductance of G. When an X-ray photon hits, the temperature of the absorber will increase and is shown as a temperature spike. A schematic illustration of this configuration with an illustrative graph is shown in figure 2.3.

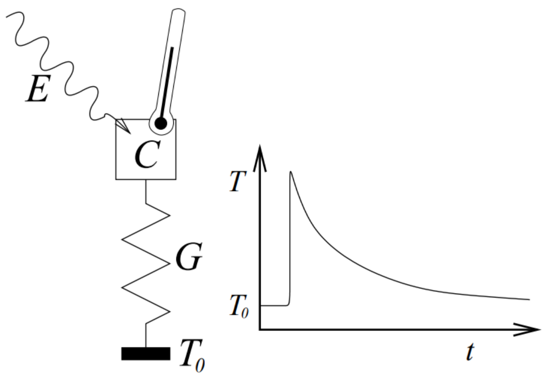

Figure 2.3: Schematic illustration of a conventional microcalorimeter. In this figure, the absorber with heat capacity C is weakly coupled with thermal inductance G to a heat bath with a temperature of T_0. When a photon with a certain energy E hits the absorber, the temperature of the microcalorimeter changes as shown in the graph on the right. [4]

2.3.1 TES electrical and thermal response

The theory described in this section finds its origin in chapter 2 of [8]. Parts related to the graduation assignment have been dissected and are presented here.

It is possible to bias a TES with either one of two ways: voltage biased or current-biased. When current-biased, it is difficult to keep the detector operating in the extremely narrow superconducting transition. This is because of Joule heating of the TES which can lead to thermal runaway and small fluctuations in bath temperature. This will also significantly degrade performance. In an array, it can even become impossible to use current-bias.

When a TES is voltage-biased, the device can easily be kept stable against thermal runaway and can be self-regulated in temperature with much less sensitivity to fluctuations in the bath temperature. One issue that voltage-biased and current biased TES-detectors suffer is that the TES is a low-impedance device (typically 100 mΩ). To maximize the signal to noise ratio, the impedance between the device and readout should match each other.

There are not that many options for amplifiers to do this which have the capability to work at low-temperature and low-impedance. To do this, in most cases, a Superconducting QUantum Interference Device (SQUID) is used which does meet these requirements.

The SQUID amplifiers are operated at low temperatures, but they are biased and read out with room-temperature electronics. Wires are run from room temperature to the operating temperature of the SQUID in order to provide a bias current, to bias the squid and to provide a feedback flux to linearize the SQUID output.

It is impossible to directly couple the output of a SQUID to a room-temperature amplifier because the output voltage would be too low. To solve this problem, a variety of techniques can be used, one of which is using a series array of SQUIDs to increase the output voltage swing [12][13][14].

A typical SQUID readout circuit for a TES is shown in figure 2.4. In this figure the TES can be seen to operate at its operating temperature of 50 mK. At the same temperature, a first-stage SQUID chip is mounted and connected by wire bonds to the TES chip. Above that, at 4K, a series-array of SQUID amplifiers amplifies the signal sufficient enough to allow coupling to room temperature electronics.

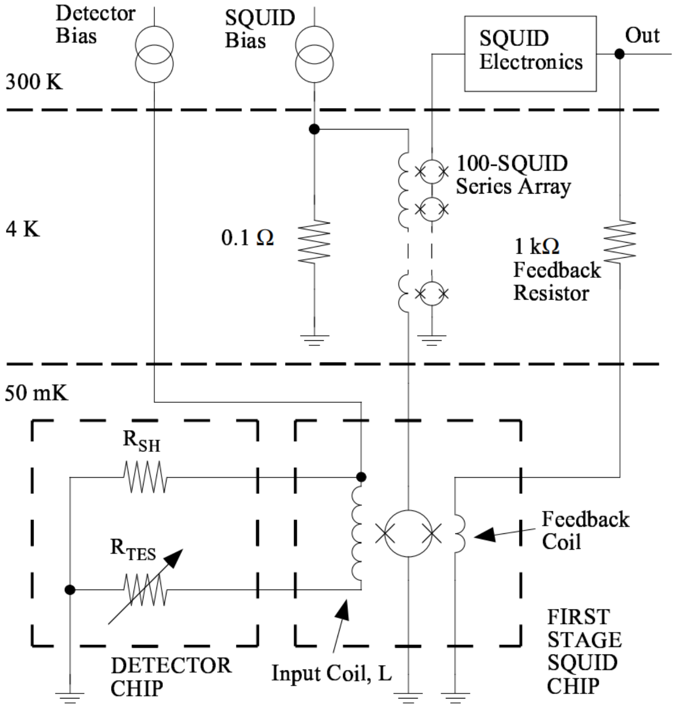

Figure 2.4: An example of a SQUID readout circuit for a TES. A TES is voltage-biased by applying a current to a small shunt resistor R_{SH} in parallel with the TES resistance $R_{TES} >> R_{SH}$. The current through the TES is measured by a first-stage SQUID, which is in turn voltage-biased by a current through a small shunt resistor with resistance $\approx 0.1\Omega$. The output current of the first-stage SQUID is measured by a series-array SQUID. A feedback flux is applied to linearize the first-stage SQUID. [8]

As can be seen from the figure, the bias circuit has a shunt resistance R_{SH} in series with the SQUID input coil. Besides the shunt resistance, there can also be a parasitic resistance R_{PAR} present in series with the input coil of the SQUID. When this circuit is represented by a Thevenin-equivalent it will consist of a bias circuit with a voltage $V = I_{BIAS}R_{SH}$ applied to a series combination of load resistor $R_L = R_{SH} + R_{PAR}$, the SQUID inductance L, and the TES. The Thevenin-equivalent circuit is shown in figure 2.5.

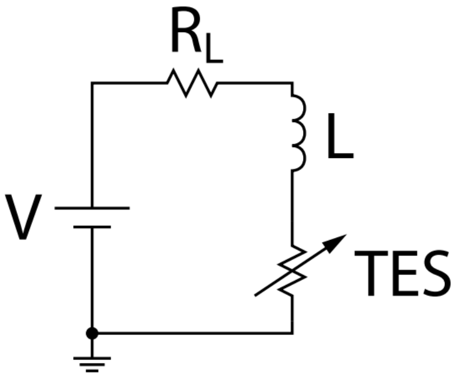

Figure 2.5: The Thevenin equivalent of the circuit in figure 2.4. In this circuit, a voltage bias $V = I_{\mathtt{BIAS}} R_{\mathtt{SH}}$ is applied to a load resistor $R_{\mathrm{L}} = R_{\mathtt{SH}} + R_{\mathtt{PAR}}$, the inductance L, and the TES. [8]

The response of the TES is governed by two differential equations which describe the electrical en thermal circuits. The electrical equation determines the current I, and the thermal equation determines the temperature T. When noise terms are ignored, the thermal equation is given by equation 2.1.

$$C\frac{\mathrm{d}T}{\mathrm{d}t} = -P_{\mathrm{bath}} + P_{\mathrm{J}} + P \tag{2.1}$$

In which:

C	Heat capacity of TES absorber	$(\mathrm{J{\cdot}K^{-1}})$
$\mathrm{d}T$	Change in TES temperature	(K)
$\mathrm{d}t$	Elapsed time	(s)
P_{bath}	Power flowing from the TES to the heat bath	$(\mathrm{J{\cdot}s^{-1}})$
P_{J}	Joule power dissipation	$(\mathrm{J{\cdot}s^{-1}})$
P	Signal power	$(\mathrm{J{\cdot}s^{-1}})$

Again ignoring noise terms, the electrical equation is given by:

$$L\frac{\mathrm{d}I}{\mathrm{d}t} = V - IR_{\mathrm{L}} - IR(T,I) \tag{2.2}$$

In which:

L	Inductance of the SQUID input coil	(H)
$\mathrm{d}I$	Change in electrical current	(A)
$\mathrm{d}t$	Elapsed time	(s)
V	Thevenin-equivalent bias voltage	(V)
I	Electrical current through TES	(A)
R_{L}	Thevenin-equivalent load resistance	(Ω)
$R(T,I)$	Electrical resistance of TES	(Ω)
T	Temperature of TES	(K)

The two differential equations are complicated by several nonlinear terms but can be linearized in a small-signal limit assumption around the steady-state values for resistance, temperature and current: R_0, T_0, I_0. For small signals, the resistance of the TES can be expanded around these steady-state values. The electrical resistance of the TES in the first order is then given as:

$$R(T,I) \approx R_0 + \left.\frac{\partial R}{\partial T}\right|_{I_0} \delta T + \left.\frac{\partial R}{\partial I}\right|_{T_0} \delta I \tag{2.3}$$

In which:

R	Resistance of the TES	(Ω)
R_0	Steady state resistance	(Ω)
I_0	Steady state current	(A)
T_0	Steady state temperature	(K)

In this equation, δT is equal to the difference between the measured temperature and the steady-state temperature; $\delta T = T - T_0$. δI is equal to the difference between the measured current and the steady-state current; $\delta I = I - I_0$.

The unitless logarithmic temperature sensitivity of the TES is given by the variable α_I;

$$\alpha_I \equiv \left.\frac{\partial \log(R)}{\partial \log(T)}\right|_{I_0} = \left.\frac{T_0}{R_0}\frac{\partial R}{\partial T}\right|_{I_0}, \tag{2.4}$$

and the unitless current sensitivity by β_I;

$$\beta_I \equiv \left.\frac{\partial \log(R)}{\partial \log(I)}\right|_{T_0} = \left.\frac{I_0}{R_0}\frac{\partial R}{\partial I}\right|_{T_0}. \tag{2.5}$$

Combining equations 2.2, 2.4 and 2.5 gives the expression for the resistance which is equal to:

$$R(T,I) \approx R_0 + \alpha_I \frac{R_0}{T_0}\delta T + \beta_I \frac{R_0}{I_0}\delta I \tag{2.6}$$

In which:

α_I	The thermal sensitivity	(-)
β_I	The current sensitivity	(-)

2.3.2 Circuit noise and energy resolution prediction

The TES suffers from a variety of noise sources such as phonon noise, Johnson noise, shunt resistor noise and noise from other circuit components. Each of these noise sources has its own spectral noise density which can be calculated [8][15]. This noise density can be translated to a noise equivalent power (NEP) for that specific noise source. If all noise sources are known, the total NEP can be calculated by adding all the spectral noise density components and taking the square root of it [8].

If the NEP is found and optimum filtering [16] is used, a theoretical FWHM energy resolution can be calculated [14]. This theoretical value for the energy resolution is given by:

$$\Delta E = 2.36\xi\sqrt{k_{\mathrm{B}}T^2C} \tag{2.7}$$

with;

$$\xi = 2\sqrt[4]{\gamma\left(\frac{1}{\alpha L_0} + \frac{G}{G_{\mathrm{TES}}}\right) + \left(\frac{1}{\alpha L_0} + \frac{G}{G_{\mathrm{TES}}}\right)^2} \tag{2.8}$$

In which:

ΔE	Theoretical energy resolution of TES	(eV)
k_{B}	Boltzmann constant	($\mathrm{m^2 \cdot kg \cdot s^{-2} \cdot K^{-1}}$)
T	TES temperature	(K)
C	Heat capacity of TES absorber	($\mathrm{J \cdot K^{-1}}$)
γ	Thermal gradient	(-)
α	Steepness of the transition	($\mathrm{K \cdot \Omega}$)
L_0	Loop gain	($\mathrm{V^2 \cdot W^{-1} \cdot K^{-1}}$)
G	Dynamic thermal conductance to the bath	($\mathrm{W \cdot K}$)
G_{TES}	Internal thermal conductance of the TES	($\mathrm{W \cdot K}$)

This equation is only valid for the small-signal limit of the TES. For bigger signals, multiple non-linear terms are added and this equation is no longer valid. However, it does give an idea as to which parameters are important to tune in order to achieve a high energy resolution.

2.4 Superconducting Quantum Interference Device (SQUID)

A TES has a extreme sensitivity to measure small energy changes. However, this small energy change causes a small signal which can not be detected by a detector. Therefor, the signal has to be amplified. This is done with the use of a so called SQUID, which stands for Super Conducting Quantum Interference Device. These SQUIDS are made out of a ring broken up in two places to create Josephson junctions. These Josephson junctions cause interference between each other and a will produce a high current when a small change in magnetic field is incident. [17]

For the SQUID to amplify a signal without noise, it is important for the phase of the SQUID to be locked. If this is not the case, then the phase in the SQUID will oscillate. When the SQUID is placed in a phase locking circuit, it is also called a phase-locked loop. [17]

2.5 Josephson junctions

Josephson junctions are made by sandwiching a thin layer of a non superconducting material between two superconducting materials, also called a weak link. When this is done, pairs of superconducting electrons (cooper pairs) can tunnel through this barrier without any resistance. At least, until a critical current I_j is reached.

When the current exceeds the critical current, a voltage will start to oscillate across the junction. The frequency of this oscillation is given by equation 2.9. [18]

$$f_{\text{Josephson}} = \frac{2e\Delta V}{h} \tag{2.9}$$

In which:

$f_{\text{Josephson}}$	Oscillation frequency Josephson junction	(Hz)
e	Elementary charge	(C)
ΔV	DC voltage across junction	(V)
h	Planck constant	($\text{m}^2{\cdot}\text{kg}{\cdot}\text{s}^{-1}$)

The oscillation frequency of the Josephson junction is less than the applied AC-bias frequency to the circuit. For this reason, weak-link oscillations in the response of the TES are present.

2.6 Multiplexing

TES microcalorimeters have a high energy resolution because of their sharp transition region at low temperature. However, before any signal can be read out by room temperature electronics, the signal has to be amplified by a SQUID. The drawback of these SQUIDS is that they generate heat. Every single TES would need a SQUID to amplify its signal but this is impossible because the system in the space application would not be able to compensate for the heat generated. The TES microcalorimeters would not be able to stay stable in their transition region because of this.

To solve the problem of SQUIDS heating the array too much, so called multiplexing technique is used. There are two multiplexing techniques, time division multiplexing (TDM) and frequency division multiplexing (FDM). The one used in the measurement setup in this thesis is frequency division multiplexing.

FDM allows a single SQUID to be used for multiple TES microcalorimeters. The way this works is by giving each TES its own frequency by connecting it to an LC-resonator that has a specific resonance frequency. These frequencies have to be separated adequately from the frequencies of the other LC-resonators to prevent cross-talk. After amplification, the signal can be demodulated back into its separate channels. An illustration of how a signal is combined in FDM is shown in figure 2.6.

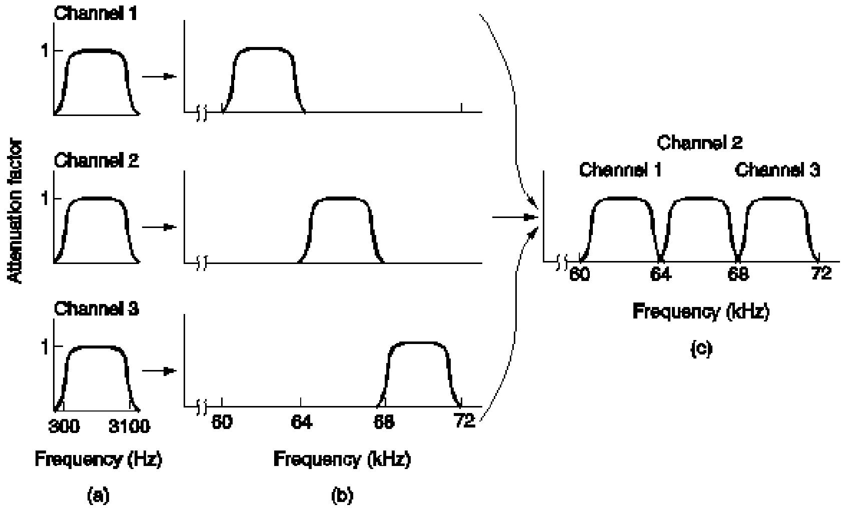

Figure 2.6: Illustrative image of how frequency domain multiplexing is done. At (a) the original signals are seen which get placed at a specific frequency in (b). In (c) the signals are combined and create a multiplexed channel. [19]

2.7 RLC-circuits

An RLC circuit is an electrical circuit which consists of three basic components; namely a resistance, inductance and capacitance. Each of these components has a different phase relationship to each other when connected to an AC power supply [20]. This phase difference depends on the frequency. When the inductive and capacitive reactances are equal but cancel each other because they are 180 degrees apart, the circuit will exhibit no resistance through these two components. The circuit will then be in resonance and only the resistance R will be seen by any applied bias voltage.

The resonant frequency of a series RLC circuit is given by equation 2.10. The Q-factor of the circuit is determined by the sharpness of the peak at the resonance frequency of the LC-components. It is given by equation 2.11. [21]

$$f_{\text{res}} = \frac{1}{2\pi\sqrt{LC}} \tag{2.10}$$

$$Q = \frac{2\pi f_{\text{res}} L}{R} \tag{2.11}$$

In which:

f_{res}	The resonance frequency of the LC-resonator	(Hz)
L	Inductance	(H)
C	Capacitance	(F)
R	Resistance	(Ω)
Q	Quality factory	(-)

3

Methods

In this chapter the work approach in working with the measurement setup is given. The measurement setup is described and the different steps taken in doing measurements is explained.

3.1 XFDM measurement setup

For this internship, the XFDM setup of SRON is used. This setup involves around a 64-pixel TES array of which 15 pixels are connected. These pixels are connected to LC-resonators on an LC-filter chip to give them an independent frequency and allow for Frequency Domain Multiplexing (FDM). All connected pixels have an absorber and are close to identical. The TES array is shown in figure 3.1 and the LC-filter chip in figure 3.2.

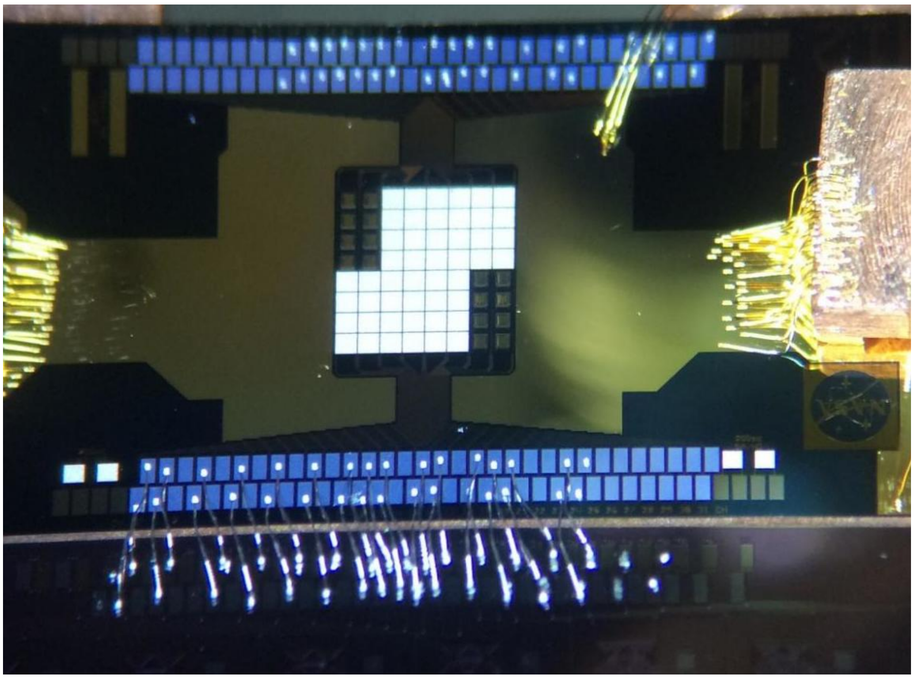

Figure 3.1: TES array. A 64-pixel TES array is shown of which 15 pixels are connected for readout under Frequency Domain Multiplexing (FDM). [22]

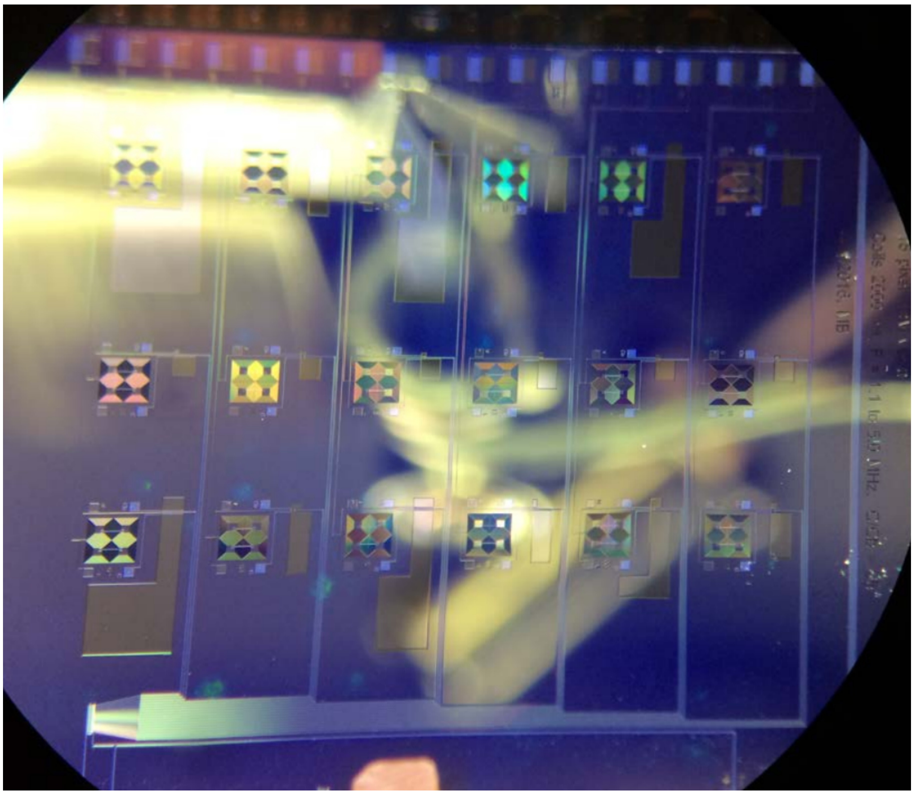

Figure 3.2: LC-filter chip. This chip contains LC-filters for the TES array pixels. Each LC-filter has its own resonance frequency, allowing each pixel to be read out under Frequency Domain Multiplexing (FDM). [22]

3.1.1 Electronics

A simplified version of the electronic circuit used to readout the TES pixels is shown in figure 3.3. The electronic circuit consists of two lines, which are the AC-bias line (ACB-line) and Feedback-line (FB-line). The ACB-line is used to put a voltage bias across the TES and is also used to give the pixel a specific frequency under which it can be read out. The frequency under which the TES is biased is determined by the resonance frequency of the LC-resonator present in the ACB-line. This ACB-line is repeated at the summing point for the other pixels of which each has a different resonance frequency.

The FB-line is used for the amplification of the signal. When a current runs through the ACB-line, a current will pass through the Input coil, causing a magnetic field to run through the FE-SQUID. This magnetic flux is cancelled by the magnetic field produced from the Feedback coil. The ratio between these two coils determines the amplification factor of the SQUID.

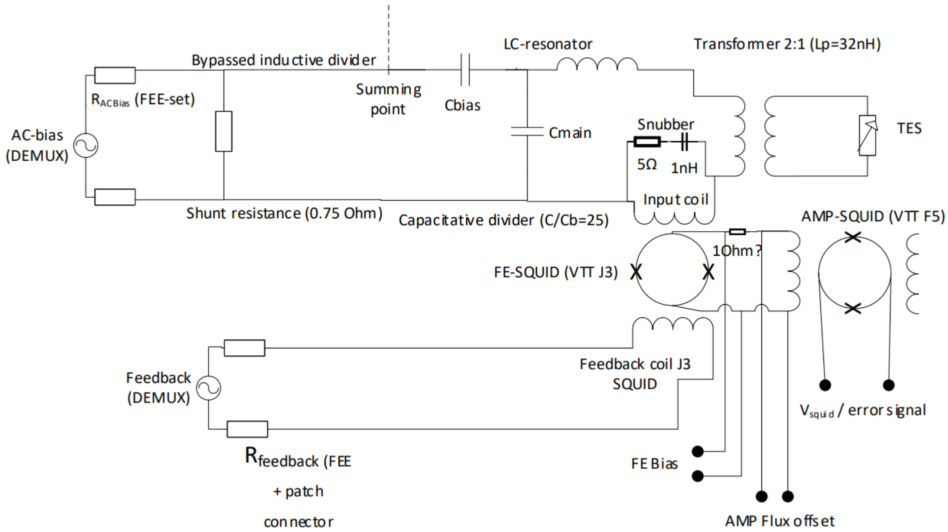

Figure 3.3: Circuit diagram of the LC-resonators and TES between AC-bias and FE-SQUID. [22]

The LC-resonators are put in to make Frequency Domain Multiplexing (FDM) possible. Each of the pixels in the TES array has its own LC-resonator circuit connected which allows all of the pixels to be amplified using only one SQUID. By tuning into the right frequency, each pixel can be read out at the same time using this configuration.

One of the reasons it is necessary to use FDM is that connecting all of the pixels to their own independent SQUID would greatly amplify the heat generated. Because the instrument in the Space application has a limited supply of electrical power, the cooling power of the coolers is severely limited. For this reason, multiplexing technology is necessary.

3.1.2 The cryogenic dilution refrigerator

The TES microcalorimeters on the XFDM setup have an operating temperature at a sub-kelvin level of 50 mK. To reach such low temperatures, a cryogenic dilution refrigerator is used. This refrigerator consists of multiple cooling stages of which the lowest cools down to sub-kelvin levels using 4He and 3He dilution process. Details on how this process works can be found in Appendix 1.

The cooler itself is shown in figure 3.4. The different cooling stages can be seen and their temperatures. On the bottom plate of the refrigerator, the measurement setup which is used in the graduation internship is located.

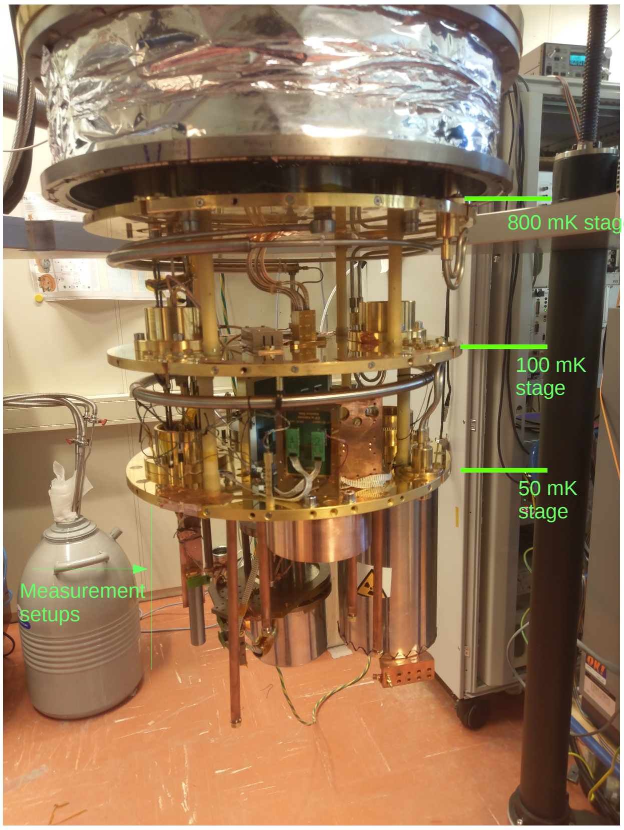

Figure 3.4: The cryogenic dilution refrigerator. In this picture, the different cooling stages of the setup are shown. The lowest stage contains the measurement setups used for a variety of experiments. The TES array is also located on this bottom stage.

3.1.3 X-ray source

To simulate X-ray photons that hit the detector from outer space, an X-ray source is used in the measurement setup. This source is a Fe-55 source of which the energy of the incoming radiation is known with high accuracy. Using this source, it is possible to evaluate the system and to determine the energy resolution of the TES microcalorimeters.

An example of the obtained spectrum from the Fe-55 source is shown in figure 3.5. In this figure, the two characteristic Kα_1 and Kα_2 lines can be seen at respectively 5.89875 keV and 5.88765 keV [23]. The relative probability of the Kα_2 emission is about half of that of the Kα_1. For this reason, the amount of counts for this Kα_2 peak is half of that of the Kα_1 peak. The spectrum shown in the figure was obtained using pixel 0 at a frequency of 1068.25 kHz using a bias voltage of 140 mV in the XFDM measurement setup.

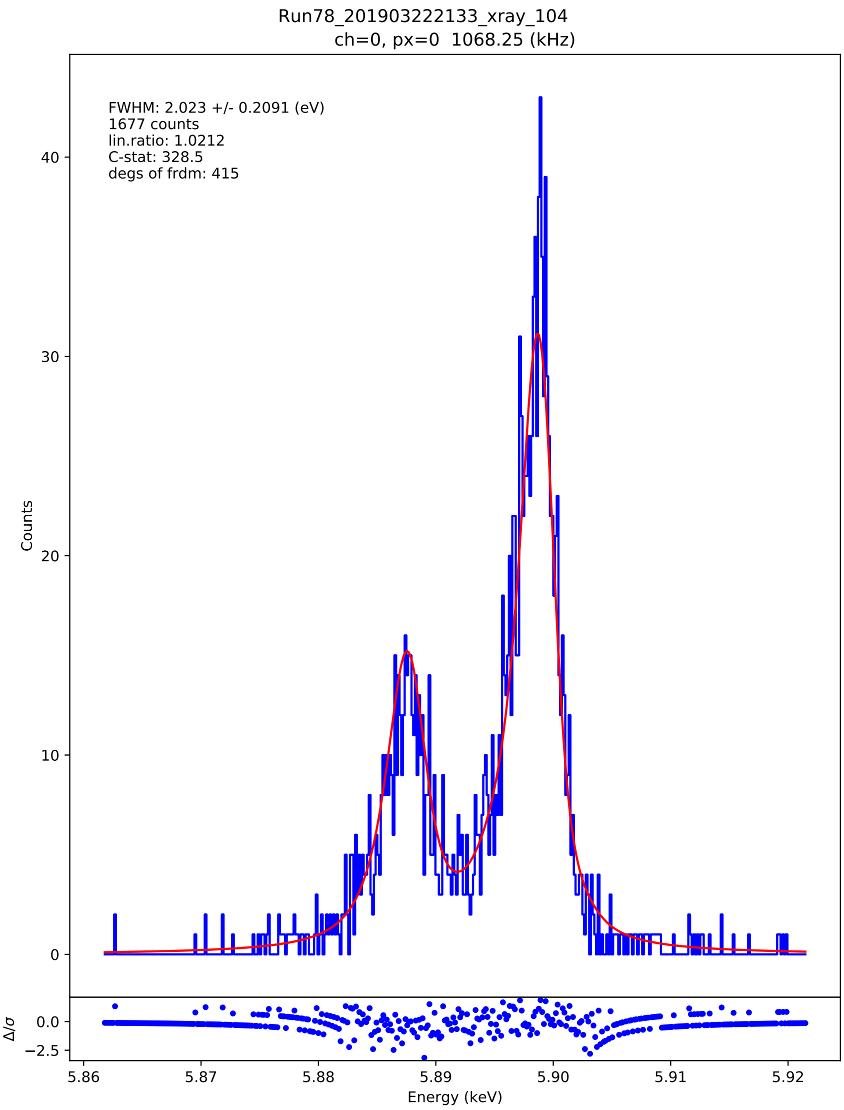

Figure 3.5: Spectrum measurement of the Fe-55 source using the TES microcalorimeter at pixel 0 in the XFDM measurement setup. From this measurement, an energy resolution of 2.02 eV with a one sigma error of 0.2 eV was obtained.

3.2 Taking measurements

In order to find correlations between the X-ray energy resolution and any of the TES properties, it is necessary to understand how the measurements are done and how they are linked together.

3.2.1 Determining X-ray energy resolution

To obtain the X-ray energy resolution, a measurement is taken in which the TES is bombarded by X-ray photons coming from the Fe-55 source. The energy of these photons is well known and create, as previously stated, two peaks at 5.88765 keV and 5.89875 keV [23]. The width of these peaks is well known from the literature. The performance of the detector causes the peaks to convolve. The level of how much they convolve is determined by the full width at half maximum. This value is what defines the X-ray energy resolution of the detector.

The resolution measurement can take some time depending on the count rate of the Fe-55 source. The Fe-55 source used in the measurement setup has a count rate of around 0.7 photons per second. To obtain reasonable results with low error margins the number of counts received is very important. To obtain a one sigma error of 0.2 eV, it is necessary to have around 3500 photon counts. The error follows a Poisson distribution, so if the error has to be twice times smaller, the amount of counts received has to increase a factor of four.

Because determining the energy resolution takes so long, other methods in determining the optimum operating conditions are searched for in the TES and circuit characteristics. However, to verify if these methods are successful these long measurements still have to be taken.

3.2.2 TES characteristics

When putting a voltage across the TES, a current will start to flow through it. This current depends on the resistance of the TES. It increases linearly with voltage except for when the TES is in its transition region. By variating the voltage, the temperature of the TES can also be regulated which makes it possible to choose a specific point on the superconducting transition.

Direct measurements of the resistance of the TES are impossible. However, the current that flows through it can be measured as a function of the bias voltage. This is called an IV-curve measurement and an example of it is shown in figure 3.6.

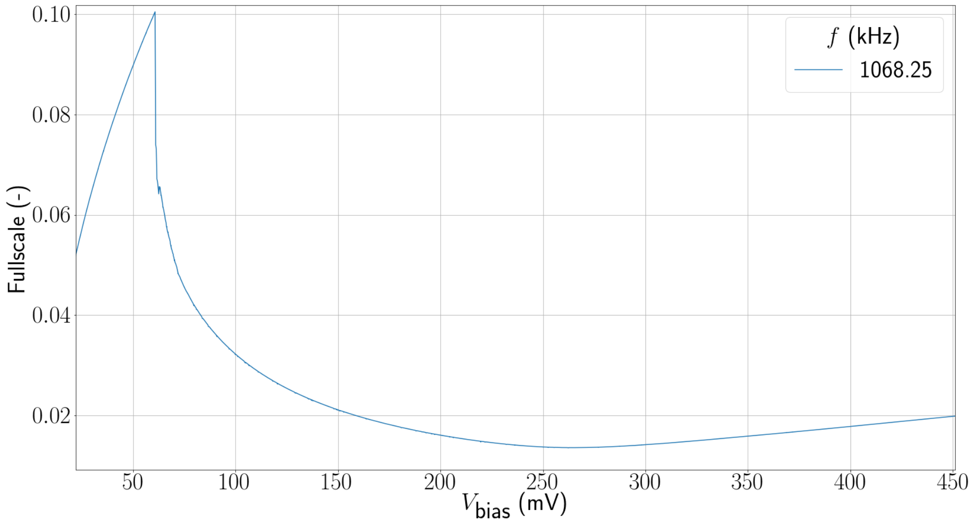

Figure 3.6: Example IV-curve for pixel 0 in the XFDM measurement setup, working at a bias frequency of 1068.25 kHz.

The phase of this IV-curve can be derived and creates the phase curve. In this curve, the weak-link effect in the superconducting transition can be seen more clearly. The phase curve of the IV-curve presented in figure 3.6 is shown in figure 3.7.

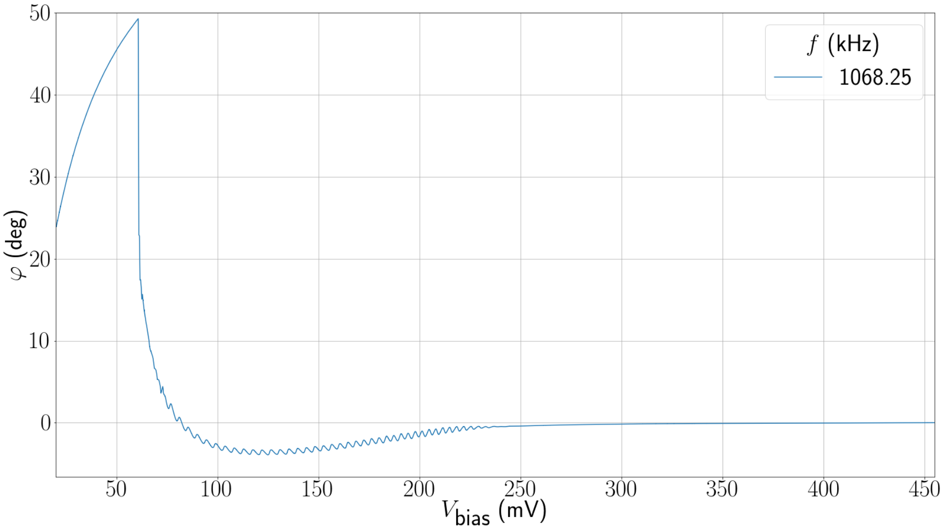

Figure 3.7: Example phase curve for pixel 0 in the XFDM measurement setup, working at a bias frequency of 1068.25 kHz.

The phase curve and IV-curve can be measured at the same time. These curves can also be measured in a few minutes which is why characteristics from these curves are searched for that could determine good energy resolutions. If correlations between these curves and the X-ray energy resolution are found, then it would greatly reduce the search time to find good values for the bias parameters.

3.2.3 Circuit properties

A measurement can be done on the circuit its AC-bias line (ACB-line) and Feedback-line (FB-line). This measures the difference between the input and output of the circuit in both cases. Using this scan, components such as the LC-resonator will cause a peak at certain frequencies which relate to the resonance frequency of the resonator. This scan can be used as an indicator as to which bias frequency to pick.

3.3 Analysing the obtained data

All data obtained from the measurements has been analysed by self-made scripts in Python 3. Also, all of the plots have been made using these scripts. These scripts are not included in this thesis or in the appendices due to their length. However, they have been a large part of the work done in the graduation internship and can be found in a GitHub repository at: `https://github.com/GerwinVerkerk/AnalysisScriptsSRON`.

4

Results

4.1 Pixel characterisation

The first measurement performed during the internship was a measurement to look at the impact of changing the AC-bias frequency and voltage on the X-ray energy resolution. For this measurement, pixel 0 was used in the XFDM measurement setup. Detailed information about this measurement can be found in Appendix 3.

A colour map was made from the measurement and is illustrated in figure 4.1. One sigma (σ) error for the measured data points is around 0.2 eV and has to be kept in mind when looking at the presented colour map.

No conclusions were made from this measurement regarding the X-ray energy resolution dependency on the frequency and voltage. The reason for this is that the bias points were chosen at random. Also, the error is too large due to the low amount of counts. Other measurements were taken to examine these correlations. What can be said from the measurement shown in figure 4.1 is that changing the frequency and voltage can change the resultant X-ray energy resolution significantly, even outside the error ranges.

It is known that, because of the LC-resonator, the frequency determines the signal the amount of signal that passes through the circuit. But how the best X-ray energy resolution relates to this LC-resonator peak was unknown. To determine this dependency, a measurement of the X-ray energy resolution as a function of the AC-bias frequency and so-called loop-gain was done. The relationship between these parameters is researched of which the results can be found in section 4.2.

The bias voltage determines at which point in transition the TES is. From the measurement shown in figure 4.1 a lot of different energy resolutions are achieved for different voltages at different frequencies. From experience, it is assumed that the voltage does not influence the X-ray energy resolution all that much as long as the TES stays low in its superconducting transition. However, the voltage also determines the slope in the phase curve. The slope could influence the X-ray energy resolution more than just the point in transition. A measurement was done to verify this and can be found in section 4.3.1.

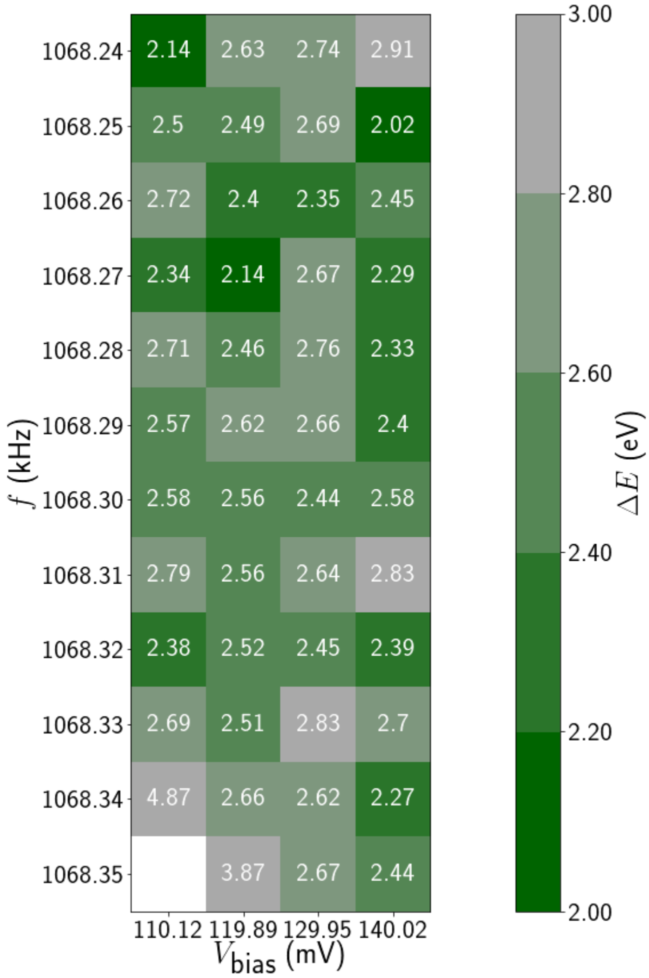

Figure 4.1: TES energy resolution as a function of the bias frequency f and voltage V_{bias}. This plot was made using pixel 0 in the XFDM setup.

4.2 Correlation between energy resolution, frequency and gain

In the first measurement of section 4.1, no conclusions were made regarding the X-ray energy resolution dependency on the AC-bias frequency. The error in the measured data was too big and the scatter too large. A new long measurement was taken to look at these parameters to check for a correlation.

Besides only looking at the X-ray energy resolution dependency on the AC-bias frequency, a Network Analyser Scan (NWA) was performed on the used pixel 0. From the NWA scan, the electrical signal that passes through the circuit is measured and is called the gain. The gain is not to be confused with amplification, because in this case, the gain represents only the ratio between the input and output signal.

The NWA scan can be performed on two lines. These are the ACB-line (AC-bias line) and the FB-line (feedback line). The feedback line is, under the operational mode, used to cancel out the flux that passes through the amplification SQUIDs. When measuring the signal through the ACB-line, a peak exists at the resonance frequency of the LC-resonator. However, when measuring the signal through the FB-line, a peak will also exist at or very close to that of the LC-resonator resonance frequency. This is because the FB-line 'sees' the LC-resonator in the ACB-line through the output coil. Also because of parasitic inductances in the FB-line, a trough exists next to the resonance peak. The distance from the peak to trough is kept as close as possible but is dependent on the AC-bias frequency under which the pixel operates for FDM. For the measured pixel 0, this distance is very close. The optimum frequency is from experience in previous measurements expected to lay between this peak and trough.

The NWA scan for the ACB-line is presented in figure 4.2. The resonance frequency f_{res} of the LC-resonator obtained from this scan lays on 1068.26 kHz. The NWA scan for the FB-line can be seen in figure 4.3. As can be seen in this figure, the resonance frequency of the LC-resonator lays close that that of the ACB-line at 1068.29 kHz. The trough is located to the left to the resonance peak.

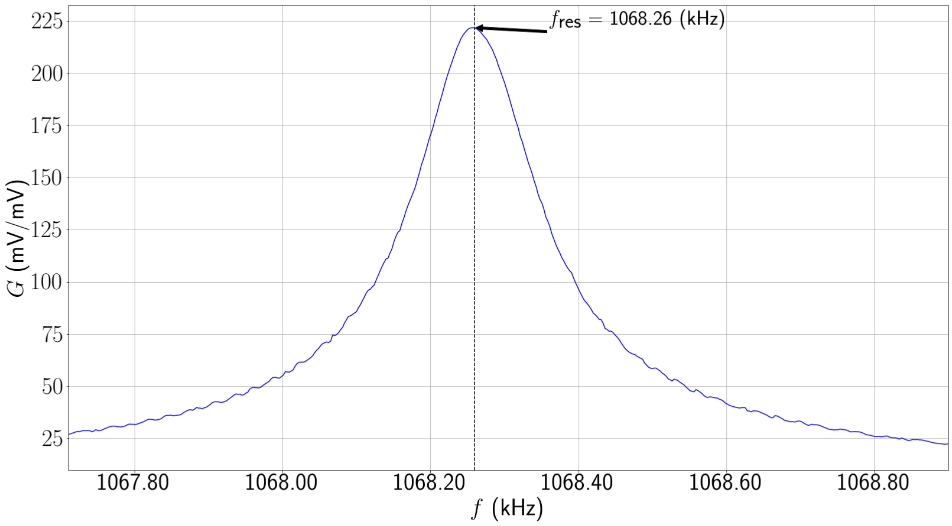

Figure 4.2: Network analyser scan for the AC-bias line. In this figure, the resonance frequency of the LC-resonator can be seen around 1068.26 kHz.

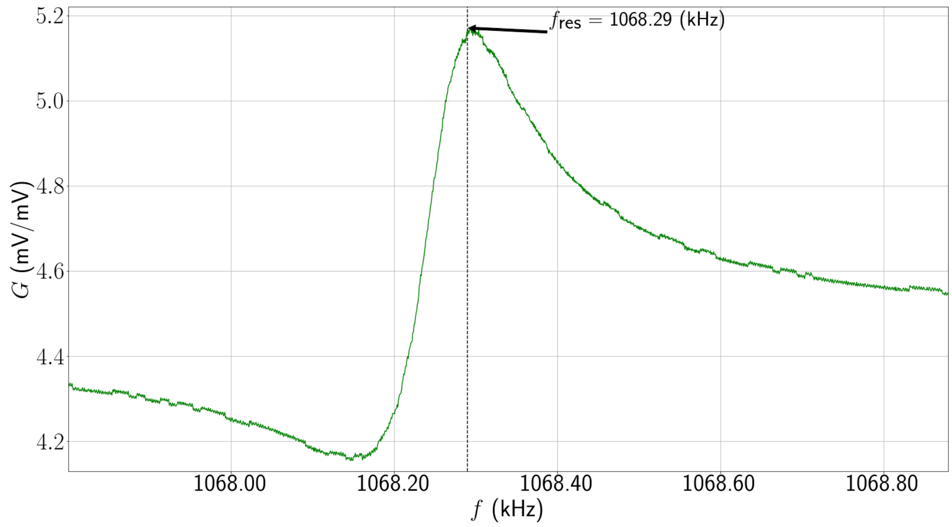

Figure 4.3: Network analyser scan for the FB-Bias line. The feedback circuit 'sees' the electrical circuit of the AC-Bias line and therefore a frequency is present close to equal to that of the LC-resonator resonance frequency. The dip is caused by the difference between the input and output coil in the electrical circuit which induces a parasitic inductance.

In the sections below, the X-ray energy resolution as a function of the AC-bias frequency and the gain of the feedback-line is given for both the Dual-FEE electronics and Single-FEE electronics. The Single-FEE electronics were introduced in a late stage of the internship due to stability issues with the Dual-FEE electronics. The main difference between the Single-FEE and the Dual-FEE is the number of channels that can be read out simultaneously. For the Dual-FEE this is equal to two and for the Single-FEE this is one. The electronics are used for biasing the TES and reading it out.

4.2.1 Dual-FEE electronics

Knowing where the resonance frequency in the FB-line is located, an X-ray resolution measurement was performed to scan the frequency range from 1068.0 kHz up to 1068.50 kHz. The result of this measurement is shown in figure 4.4. The X-ray energy resolution ΔE is plotted as a function of the AC-bias frequency f. On the right vertical axis, the gain of the NWA-scan is given and is also plotted as a function of the AC-bias frequency. The residual between the fitted line and the measured data point is given on the bottom of the graph by ζE. The measurement was performed for two bias voltages of 110 mV and 130 mV. These voltages were kept constant through the frequency scan.

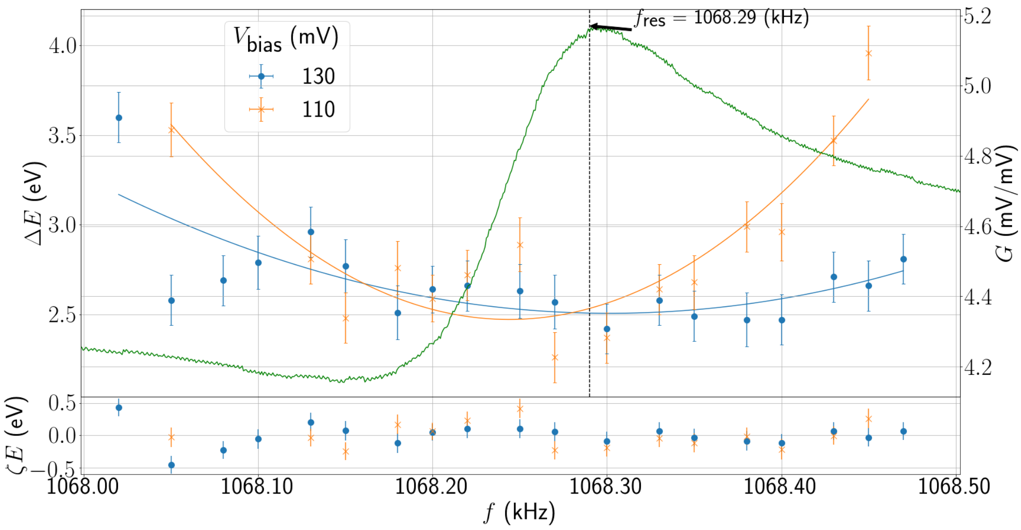

Figure 4.4: X-ray energy resolution ΔE as a function of the AC-bias frequency f. The gain G of the FB-circuit is plotted on the right vertical axis. A second order polynomial fit has been made through the data to describe the path of the data. The measurement was done at two bias voltages of 110 mV and 130 mV. The Dual-FEE electronics were used in this measurement.

Because an LC-resonator has a parabolic shape, a second-order polynomial was fitted through the obtained data points. When looking at the fits with a biased eye, one could claim they are reasonable for the given data set. To verify if this is indeed the case, the chi-squared test for goodness of fit was performed.

According to [24][25], the obtained values from the chi-squared test indicate the fit to be bad for the data set. The 130 mV line has a chi-squared value of 29.29 with 16 DoF (Degrees of Freedom) and the 110 mV has a chi-squared value of 25.37 with 12 DoF. This gives a certainty that the fit for the 130 mV line is good of less than 2.5% and for the 110 mV line of less than 2%. It can be said that the fits are bad.

4.2.2 Single-FEE electronics

All of the above measurements were done using the Dual-FEE electronics. These electronics are used for biasing the TES and reading it out. However, stability issues were present and a switch was made to the, by SRON, previously used Single-FEE electronics. The same measurement regarding the X-ray energy resolution on frequency and gain was executed using the Single-FEE electronics and is worked out below. The measurement results for this measurement are given in Appendix 5.

The energy resolution as a function of AC-bias frequency and the gain of the feedback loop for the Single-FEE electronics is shown in figure 4.5. The same fit as for the measurement results using the Dual-FEE electronics was made for the results obtained using the Single-FEE electronics.

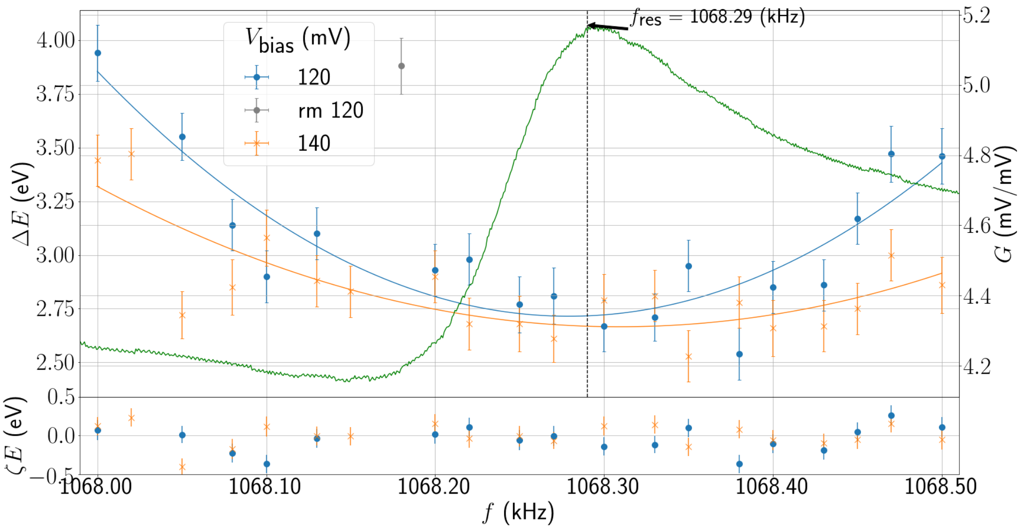

Figure 4.5: X-ray energy resolution ΔE as a function of the AC-bias frequency f. The gain G of the FB-circuit is plotted on the right vertical axis. A Gaussian fit has been made through the data to describe the path of the data. The measurement was done at two bias voltages of 120 mV and 140 mV. Outliers of more than three sigmas from the expected course of the data points are excluded from the fit and are indicated by 'rm' and greyed out. The Single-FEE electronics were used in this measurement.

Again to check the goodness of fit, the chi-squared value was calculated. For the 120 mV line, the value that came out of the calculation is equal to 28.52 and has 15 DoF. The certainty that this is a good fit is less than 2% for this line. For the 140 mV line, chi-squared is equal to 30.35 with 17 DoF and gives certainty of less than 2.5% of being good. This concludes that fitting a second-order polynomial is insufficient to describe the path of the obtained data.

4.2.3 Gaussian fit for Dual-FEE and Single-FEE

Both data gained from the Dual-FEE and Single-FEE electronics are not well described by a second-order polynomial. For this reason, other fitting methods were performed. A Gaussian fit was made as it was expected to describe the path of the data better. The result of this Gaussian fit for the Dual-FEE is shown in figure 4.6 and for the Single-FEE in figure 4.7.

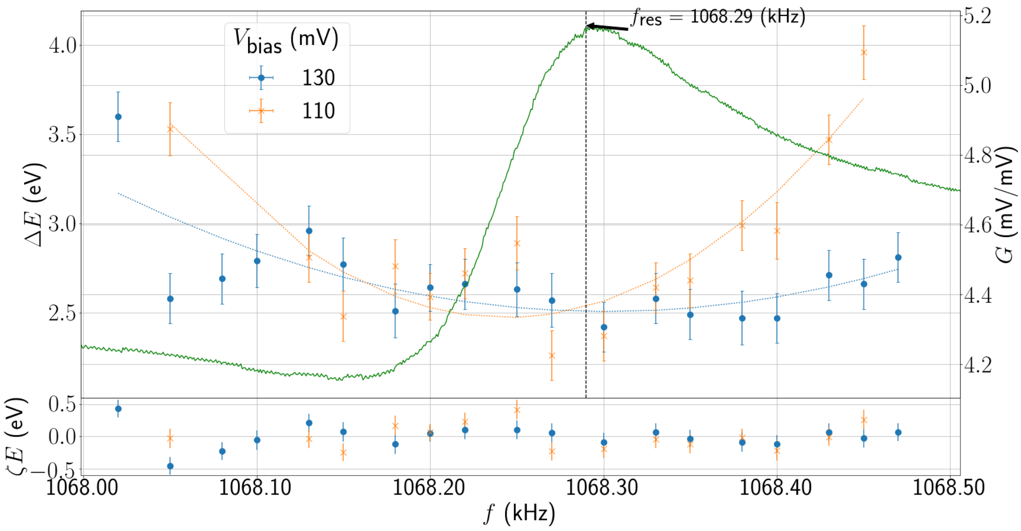

Figure 4.6: X-ray energy resolution ΔE as a function of the AC-bias frequency f. The gain G of the FB-circuit is plotted on the right vertical axis. A Gaussian fit has been made through the data to describe the path of the data. The measurement was done at two bias voltages of 110 mV and 130 mV. The Dual-FEE electronics were used in this measurement.

For the measurement using the Dual-FEE, the chi-squared value for the 110 mV line is equal to 25.4 with 11 DoF. For the 130 mV line, it is equal to 29.31 with 15 DoF. This gives the certainty [25] that these fits are good of less than 1% and 2% respectively.

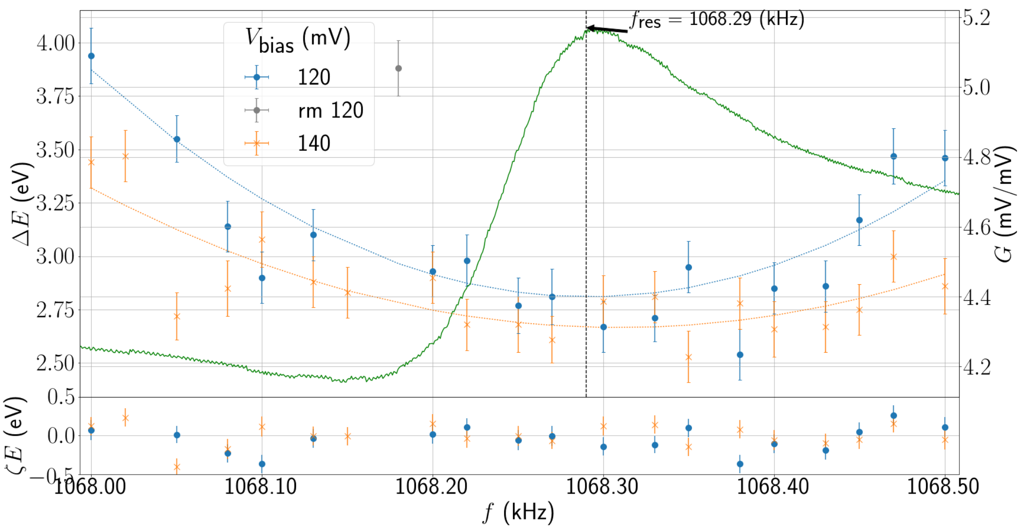

Figure 4.7: X-ray energy resolution ΔE as a function of the AC-bias frequency f. The gain G of the FB-circuit is plotted on the right vertical axis. A Gaussian fit has been made through to data to describe the path of the data. The measurement was done at two bias voltages of 120 mV and 140 mV. Outliers of more than three sigmas from the expected course of the data points are excluded from the fit and are indicated by 'rm' and greyed out. The Single-FEE electronics were used in this measurement.

For the measurement using the Single-FEE, the chi-squared value for the 120 mV line is equal to 35.23 with 14 DoF. For the 140 mV line, it is equal to 30.36 with 16 DoF. This gives the certainty [25] that these fits are good of less than 0.2% and 2% respectively.

A table that summarizes all the fits and obtained values for chi-squared is given in table 4.1. The value of P in this table gives the certainty that the fit is good.

Table 4.1: The goodness of fit for different fits determined by the chi-squared value X^2. The degree of freedom for each fit is given by DoF and the certainty of that the fit is good is given by P.

Chi-squared test for goodness of fit	X^2	DoF	P
Dual-FEE; second-order polynomial fit 130 mV line	29.29	16	0.025
Dual-FEE; second-order polynomial fit 110 mV line	25.37	12	0.020
Single-FEE; second-order polynomial fit 120 mV line	28.52	15	0.020
Single-FEE; second-order polynomial fit 140 mV line	30.35	17	0.025
Dual-FEE; Gaussian fit 130 mV line	29.31	15	0.020
Dual-FEE; Gaussian fit 110 mV line	25.40	11	0.010
Single-FEE; Gaussian fit 120 mV line	35.23	14	0.002
Single-FEE; Gaussian fit 140 mV line	30.36	16	0.020

Although the fits are unable to describe the path of the data, it has to be kept in mind that a bad fit does not mean that the data is uncorrelated. In all of the plots, significant degradation can be seen when the frequency gets off resonance with the LC-resonator resonance frequency peak. It can not be concluded whether the best frequency is at the peak, trough or in between. However, it can be concluded that picking a frequency close to the LC-resonator resonance frequency is a good strategy.

Another thing that can be seen in the plots is that for lower bias voltages the dependency on frequency increases. The energy resolution will start to form a sharper peak. This can be explained because the Q-factor of the RLC-circuit increases. When a lower voltage is applied, the TES will have lower resistance and the Q-factor will increase according to equation 2.11.

4.3 Correlation between resolution and slope

Below, the X-ray energy resolution as a function of the slope in the phase curve of the IV-curve was measured. This has been done for pixel 0 in the XFDM measurement setup. This pixel works at a relatively low frequency in AC-bias. All of the other pixels in the XFDM measurement array work at higher frequencies.

4.3.1 Low-frequency AC-bias

To measure the X-ray resolution dependency on the slope in the IV-phase curve, an X-ray measurement was done at which all parameters except for the slope were kept constant (or close to constant). The measurement was done for pixel 0 in the TES array at an AC-bias frequency of 1068.25 kHz. Bias points were kept close to each other to have minimal changes in resistance. The selected bias points on the phase curve can be seen in figure 4.8 and zoomed in up upon in figure 4.9. The resistance between these bias points changes no more than 4%. Details regarding this measurement can be found in Appendix 3.

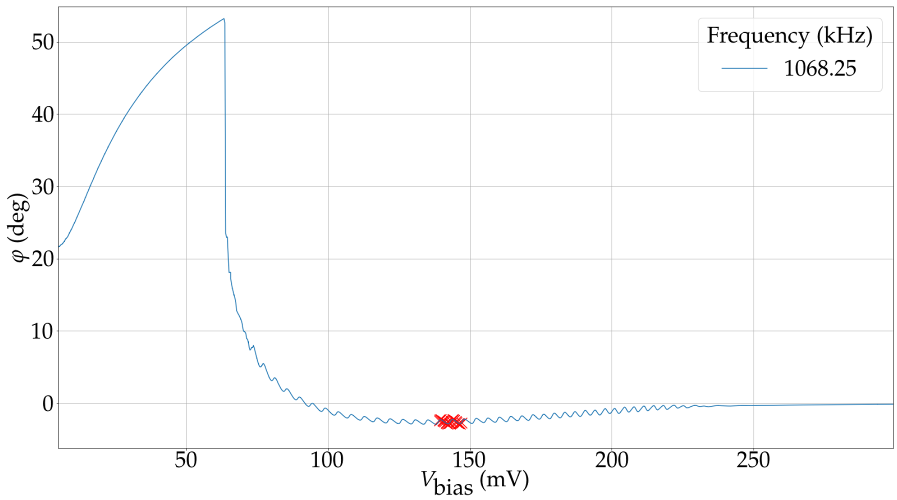

Figure 4.8: Phase curve of TES. This plot displays the phase difference φ between the input and output of the TES-circuit as a function of AC-bias voltage V_{bias}. Selected bias points on the phase curve to measure the resolution dependency on the slope. Bias points are chosen to lay close to each other as to keep the TES resistance as constant as possible.

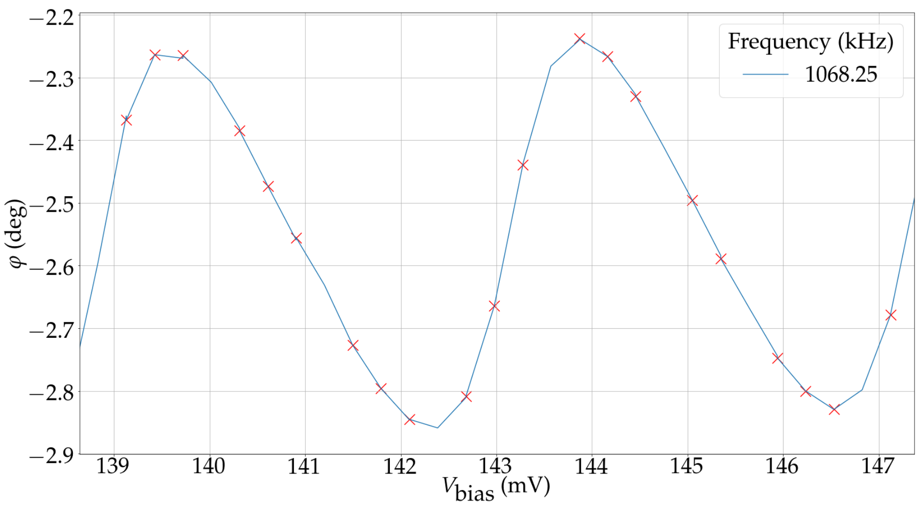

Figure 4.9: Phase difference φ between the input and output of the TES-circuit as a function of AC-bias voltage V_{bias}. Zoomed in on the selected bias points on the phase curve to measure the resolution dependency on the slope. Bias points are chosen to lay close to each other as to keep the TES resistance as constant as possible.

The slope at these bias points was obtained by taking the value of the derivative of the phase curve using a python script. The X-ray energy resolution is plotted as a function of the slope in figure 4.10.

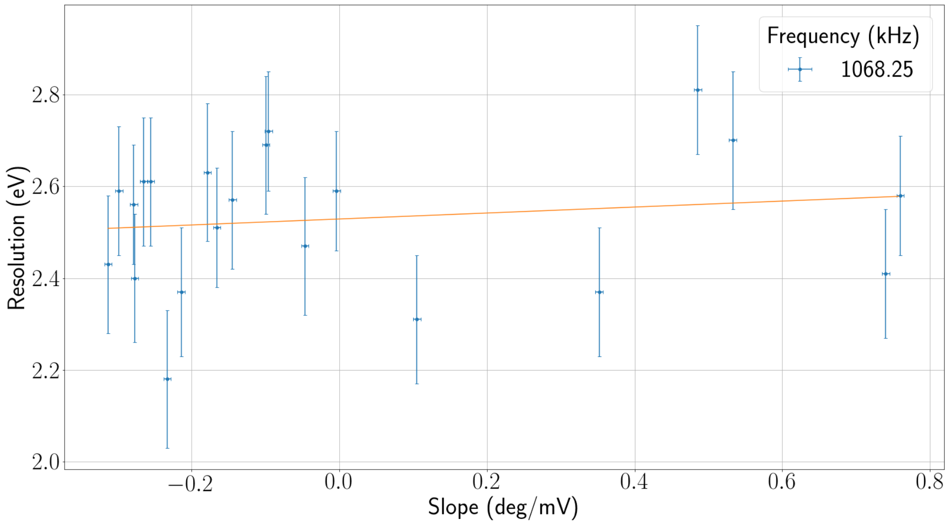

Figure 4.10: A plot of the X-ray resolution as a function of the slope in the phase curve. A linear fit was made through the data and the Pearson correlation coefficient was calculated. The estimated Pearson correlation for this fit is 0.15. In the measured region, the resistance of the TES is considered close to constant.

Before the measurements took place, it was assumed from measurement experience that a positive slope would give a better X-ray energy resolution than a negative slope. To check if this is indeed the case and if the slope in the phase curve is important, a linear fit was made through the obtained data point. A linear fit was chosen as a way to check if the resolution actually increased. The Pearson correlation coefficient [26] was calculated for the fit to see if the energy resolution got better with a positive slope. The estimated value for this Pearson correlation coefficient is equal to 0.15. However, the error in the slope is 0.52. Any correlation that would be present, is negligible [27] and victim of the error.

4.3.2 High-frequency AC-bias

High-frequency AC-bias was not measured during the internship. However, it might be possible that for higher frequencies the dependency on slope is larger. At higher frequencies, the weak link effect will cause larger phase oscillation and choosing the right bias point could become of significant importance. A discussion on this matter is found in Appendix 2.

4.4 Pixel optimisation strategy

To make a TES microcalorimeter achieve a high energy resolution, the AC-bias frequency and voltage have to be tuned. From the measurements of the X-ray energy resolution dependency on the AC-bias frequency, significant degradation is seen when the frequency gets off the resonance frequency of the LC-resonator. No fit could be made to describe the relationship between the X-ray energy resolution and the measured frequency range. However, for all measurements, both using the Single-FEE and Dual-FEE electronics, it is observed that the best X-ray energy resolutions are achieved right at or close to the resonance frequency of the LC-resonator. This means that picking a bias frequency at this LC-resonator resonance frequency is a good strategy.

The X-ray energy resolution dependency on the bias voltage has not given any determining results. The energy resolution varies significantly for different voltages but does not show a steady increase or decrease when biasing the TES at different values. The assumption that perhaps the slope in the phase curve determines the resolution has also not been proofed.

Although there does not seem to be all that significant as which bias voltage to pick, it is known that if a low voltage is picked, the TES will be low in transition. The lower in transition the TES is, the lower the resistance in the circuit will be and the bigger the Q-factor. A higher Q-factor means a sharper peak at the LC-resonator resonance frequency. It is observed that a sharper peak increases the frequency dependency on energy resolution. Thus picking a point low in transition together with a frequency close to that of the LC-resonator is a good strategy.

5

Conclusion

The X-ray energy resolution of the TES microcalorimeters depends on parameters such as the AC-bias frequency and voltage. Changing these parameter values can change the resultant X-ray energy resolution significantly.

The X-ray energy resolution is observed to be the best right at or close to the resonance frequency of the LC-resonator. This dependency gets stronger at lower bias-voltages due to the TES having a smaller resistance. This lower resistance of the TES at low bias-voltages increases the Q-factor of the RLC-circuit. A big Q-factor sharpens the peak at the LC-resonator frequency which explains the stronger X-ray energy resolution dependency on the frequency. The conclusion can be made that picking a low point in the transition, together with a frequency close to that of the LC-resonator is a good first approach strategy in obtaining a good X-ray energy resolution.

The oscillations in the phase curve of the IV-curve show a negligible correlation between their slope and the X-ray energy resolution. For pixels working at a relatively low AC-bias frequency, the slope does not seem to be an important factor for the X-ray energy resolution.

6

Discussion

It is concluded that changing the AC-bias frequency and voltage influence the X-ray energy resolution significantly. There was found no clear way to describe these correlations with a fit. The scatter is too large and a statistical relationship cannot be proofed. However, if this scatter is from a systematic effect, it can be reduced by taking repeated measurements at the same parameter values. By taking an average of such measurements, a systematic error, if present, could be removed. It could then be possible to make a fit through the data that describes and indicates the optimum frequency.

The slope in the phase curve seemed to be unimportant in giving a good energy resolution. The pixel which was used for that measurement works at a relatively low AC-bias frequency. Picking a pixel at a higher frequency will make the weak link effect cause larger oscillations. It is also known from experience that higher frequencies give worse X-ray energy resolutions, which could be linked to the larger phase oscillations. A measurement for a pixel at a higher frequency could test this hypothesis.

List of Figures

List of Tables

Bibliography

[1] SRON. Role of the institute. [Online]. Available: https://www.sron.nl/about

[2] ——. Sron's instrument science group. [Online]. Available: https://www.sron.nl/instrument-science

[3] D. Barret, T. Lam Trong, J.-W. den Herder, L. Piro, M. Cappi, J. Houvelin, R. Kelley, J. M. Mas-Hesse, K. Mitsuda, S. Paltani, G. Rauw, A. Rozanska, J. Wilms, S. Bandler, M. Barbera, X. Barcons, E. Bozzo, M. T. Ceballos, I. Charles, E. Costantini, A. Decourchelle, R. den Hartog, L. Duband, J.-M. Duval, F. Fiore, F. Gatti, A. Goldwurm, B. Jackson, P. Jonker, C. Kilbourne, C. Macculi, M. Mendez, S. Molendi, P. Orleanski, F. Pajot, E. Pointecouteau, F. Porter, G. W. Pratt, D. Prêle, L. Ravera, K. Sato, J. Schaye, K. Shinozaki, T. Thibert, L. Valenziano, V. Valette, J. Vink, N. Webb, M. Wise, N. Yamasaki, F. Douchin, J.-M. Mesnager, B. Pontet, A. Pradines, G. Branduardi-Raymont, E. Bulbul, M. Dadina, S. Ettori, A. Finoguenov, Y. Fukazawa, A. Janiuk, J. Kaastra, P. Mazzotta, J. Miller, G. Miniutti, Y. Naze, F. Nicastro, S. Scioritino, A. Simonescu, J. M. Torrejon, B. Frezouls, H. Geoffray, P. Peille, C. Aicardi, J. André, C. Daniel, A. Clénet, C. Etcheverry, E. Gloaguen, G. Hervet, A. Jolly, A. Ledot, I. Paillet, R. Schmisser, B. Vella, J.-C. Damery, K. Boyce, M. Dipirro, S. Lotti, D. Schwander, S. Smith, B.-J. Van Leeuwen, H. van Weers, N. Clerc, B. Cobo, T. Dauser, C. Kirsch, E. Cucchetti, M. Eckart, P. Ferrando, and L. Natalucci, "The ATHENA X-ray Integral Field Unit (X-IFU)," in *Space Telescopes and Instrumentation 2018: Ultraviolet to Gamma Ray*, ser. Society of Photo-Optical Instrumentation Engineers (SPIE) Conference Series, vol. 10699, Jul 2018, p. 106991G.

[4] W. M. B. Tiest, "Energy resolving power of transition-edge x-ray microcalorimeters," Ph.D. dissertation, Utrecht University.

[5] D. ir. M.T.C. de Loos-Vollebregt, *Spectrometrische analysetechnieken.* Arnhem: Syntax Media, 2009.

[6] R. Nave. Characteristic x-rays. [Online]. Available: http://hyperphysics.phy-astr.gsu.edu/hbase/quantum/xrayc.html

[7] cern. superconductivity. [Online]. Available: https://home.cern/science/engineering/superconductivity

[8] C. E. (Ed.), *Cryogenic Particle Detection.* Heidelberg: Springer, feb 2005.

[9] Hyperphysics. Fermions. [Online]. Available: http://hyperphysics.phy-astr.gsu.edu/hbase/Particles/spinc.html#c2

[10] ——. Bcs theory of superconductivity. [Online]. Available: http://hyperphysics.phy-astr.gsu.edu/hbase/Solids/bcs.html#c1

[11] ——. Superconductivity. [Online]. Available: http://hyperphysics.phy-astr.gsu.edu/hbase/Solids/scond.html

[12] R. P. Welty and J. M. Martinis, "A series array of DC SQUIDs," *IEEE Transactions on Magnetics*, vol. 27, no. 2, pp. 2924–2926, Mar 1991.

[13] ——, "Two-stage integrated SQUID amplifier with series array output," *IEEE Transactions on Applied Superconductivity*, vol. 3, no. 1, pp. 2605–2608, Mar 1993.

[14] M. E. Huber, P. A. Neil, R. G. Benson, D. A. Burns, A. F. Corey, C. S. Flynn, Y. Kitaygorodskaya, O. Massihzadeh, J. M. Martinis, and G. C. Hilton, "DC SQUID series array amplifiers with 120 MHz bandwidth (corrected)," *IEEE Transactions on Applied Superconductivity*, vol. 11, no. 2, pp. 4048–4053, Jun 2001.

[15] W. Bergmann Tiest, M. Bruijn, H. Hoevers, P. de Korte, J. van der Kuur, and W. Mels, "Understanding TES microcalorimeter noise and energy resolution," *Nuclear Instruments and Methods in Physics Research A*, vol. 520, no. 1-3, pp. 329–332, Mar 2004.

[16] E. Figueroa-Feliciano, B. Cabrera, A. Miller, S. Powell, T. Saab, and A. Walker, "Optimal filter analysis of energy-dependent pulse shapes and its application to tes detectors," *Nuclear Instruments and Methods in Physics Research Section A: Accelerators, Spectrometers, Detectors and Associated Equipment*, vol. 444, no. 1, pp. 453 – 456, 2000. [Online]. Available: http://www.sciencedirect.com/science/article/pii/S0168900299014345

[17] J. Clarke and A. I. B. (Eds.), *The SQUID Handbook*. WILEY-VCH Verlag GmbH & Co. KGaA, vol. Vol. I Fundamentals and Technology of SQUIDs and SQUID Systems.

[18] P. Müller and A. Ustinov, *The Physics of Superconductors - Introduction to Funamentals and Applications*. Springer, 1997.

[19] C. Doc. RNDr. Peter Mederly. Frequency division multiplexing. [Online]. Available: https://fmfi-uk.hq.sk/Informatika/Distribuovane%20Systemy/knihy/ICN/ch2s4p2.htm

[20] E. Tutorials. Series rlc circuit analysis. [Online]. Available: https://www.electronics-tutorials.ws/accircuits/series-circuit.html

[21] H. Physics. Selectivity and q of a circuit. [Online]. Available: http://hyperphysics.phy-astr.gsu.edu/hbase/electric/serres.html

[22] K. Ravensberg, "Wirebonding overview: Xfdm setup run 74," SRON, Tech. Rep., 2018.

[23] LNHB. Fe-55 tables. [Online]. Available: http://www.nucleide.org/DDEP_WG/Nuclides/Fe-55_tables.pdf

[24] Hinkle, Wiersma, and Jurs. Chi-square test for goodness of fit. [Online]. Available: http://www.phy.ilstu.edu/slh/chi-square.pdf

[25] medcalc. Values of the chi-squared distribution. [Online]. Available: https://www.medcalc.org/manual/chi-square-table.php

[26] L. Statistics. Pearson product-moment correlation. [Online]. Available: https://statistics.laerd.com/statistical-guides/pearson-correlation-coefficient-statistical-guide.php

[27] P. AHAMMAD. (2016, nov) How to interpret correlation coefficients. [Online]. Available: http://www.parvez-ahammad.org/blog/how-to-interpret-correlation-coefficients

Appendix 1

Cooling by helium dilution

Cooling by helium dilution Cooling to sub-kelvin levels is done through a process in which two stable isotopes of Helium, namely 4He and 3He are mixed. When these isotopes are brought together at a temperature of below 870 mK [1], a spontaneous phase separation occurs to form a 3He-rich phase and a 3He-poor phase. This happens because of nature, which does not allow certain concentration levels of 3He/4He to exist. The phase diagram illustrating this forbidden region is given in figure 1. [2]

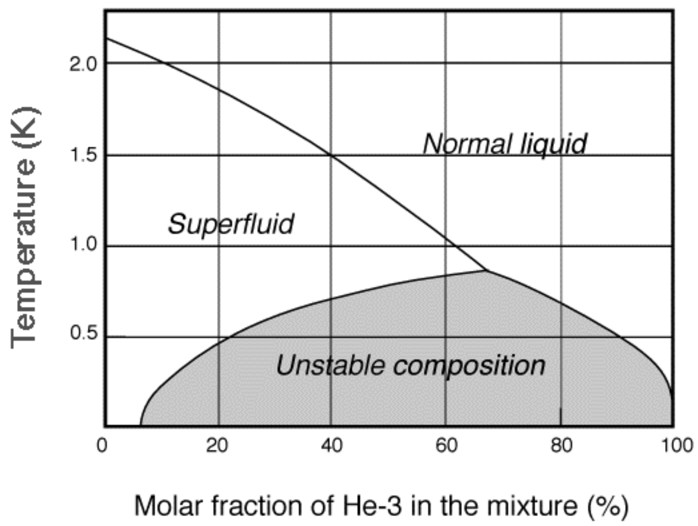

Figure 1: Phase diagram for the mixture of helium isotopes 3He and 4He. In this figure, the forbidden concentration region at temperatures below 870 mK is illustrated. [3]

The 3He-rich phase will float on top of the 3He-poor phase, since the 3He-poor phase contains mostly 4He and therefore has a higher density than the 3He-rich phase. When 3He is evaporated from the 3He-poor phase, the phase goes into the forbidden concentration region. Because this is not allowed, the 3He-poor phase will try to pull 3He from the 3He-rich phase. For this energy is needed which the 3He-poor phase gets from the walls of the dilution chamber. The energy extracted from the walls cools the walls down and thereby gives the refrigerator its cooling power. [2]

References

[1] J. Zhang, *Transport Studies of the Electrical, Magnetic and Thermoelectric properties of Topological Insulator Thin Films.* Springer, 2016.

[2] Berkeley. (2002, may) 3he-4he dilution explanation. [Online]. Available: http://cdms.berkeley.edu/UCB/75fridge/inxsrc/dilution/

[3] E. Thuneberg. (2003) Liquid mixture of 3he and 4he. [Online]. Available: http://ltl.tkk.fi/research/theory/mixture.html

Appendix 2

Netherlands Institute for Space Research

Low frequency AC-bias TES X-ray resolution dependency on slope in IV phase curve

XFDM pixel 0 at 1068.25 kHz

Graduation project Applied Physics

Measurement Report

Executed By:
Gerwin Verkerk
BSc student at The Hague
University of Applied Sciences

Date: 05-04-2019
Department: Instrument Science

1 Goal of measurement

The goal of this measurement is to find a correlation between X-ray energy resolution and any of TES properties. In this report, a correlation between the slope in the IV phase curve of a TES and X-ray resolution is looked for. For this pixel 0 in the XFDM measurement setup of SRON is used. This pixel works at a relatively low frequency in AC-bias of 1068.25 kHz.

2 Measurements

Before the measurements in this section took place, the energy resolution of the TES was measured at a specific range of bias frequencies ranging from 1068.24 kHz up to 1068.35 kHz, using 0.01 kHz step size. For each of these frequencies, four different bias points were selected at 110 mV, 120 mV, 130 mV and 140 mV. In these measurements, a correlation between bias frequency, bias voltage and energy was looked for. However, no direct correlation was found between any of the given parameters.

2.1 Expected results

Superconducting transition edge sensors behave as weak links and oscillations in their transition are present. These oscillations cause regions of non-linearity. A new hypothesis was set up that perhaps, these oscillations influence the X-ray energy resolution. If this is correct, then the slope is an important parameter to tune when a high energy resolution is desired.

If the energy resolution of a TES is dependent on the slope, then it is expected to be highest when working in a region where this slope has a high value. A high value of slope would indicate a region in the transition which approaches linearity. The TES is expected to be most sensitive there since small temperature changes would create big changes in resistance depending on how steep the slope is. The dependency is expected to be linear.

2.2 Results

A long measurement was done for a specific frequency of 1068.25 kHz. For this frequency, voltage bias points close to each other were selected. The reason for this is to keep the resistance of the TES roughly constant across all measurement points. The voltage bias points correlate to slopes going both upwards and downwards in the phase curve of the TES. The selected points in the phase curve are shown in figure 1 and are zoomed in up on in figure 2.

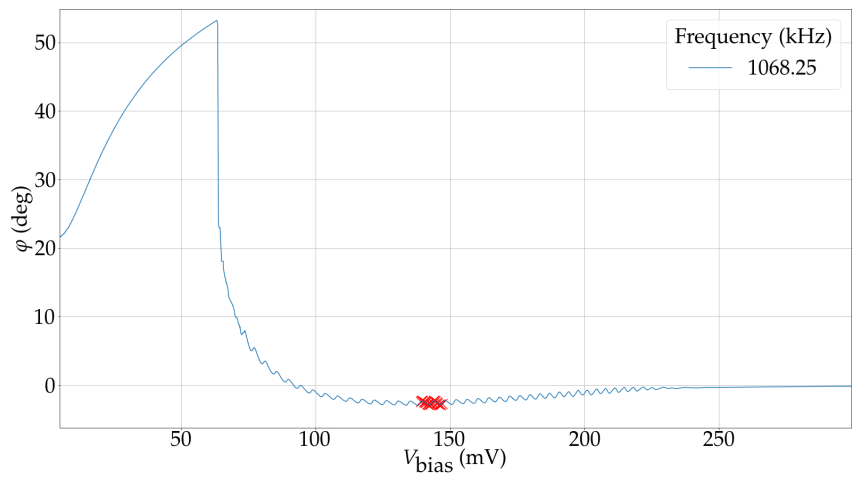

Figure 1: Phase difference φ between the input and output of the TES-circuit as a function of AC-bias voltage $V_{\mathtt{bias}}$. Selected bias points on the phase curve to measure the resolution dependency on the slope. Bias points are chosen to lay close to each other as to keep the TES resistance as constant as possible.

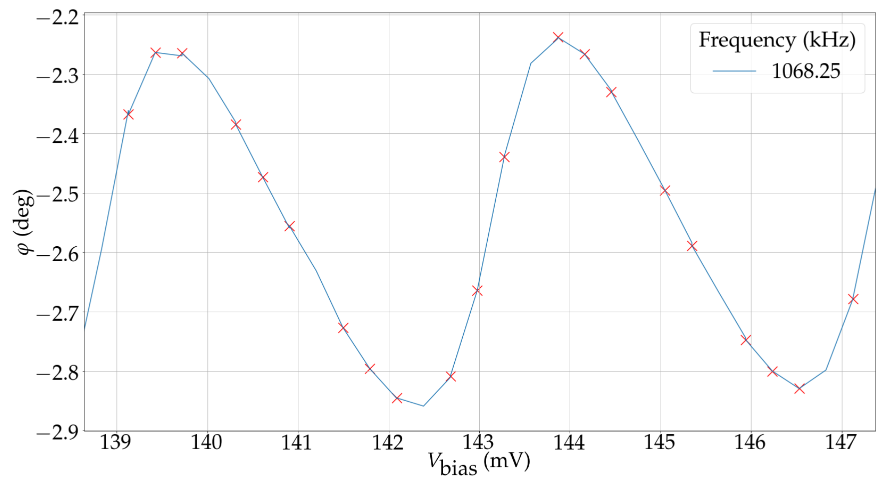

Figure 2: Phase difference φ between the input and output of the TES-circuit as a function of AC-bias voltage $V_{\mathtt{bias}}$. Zoomed in on the selected bias points on the phase curve to measure the resolution dependency on the slope. Bias points are chosen to lay close to each other as to keep the TES resistance as constant as possible.

The resistance R of the TES changes no more than 4% relative to its normal resistance R_n when measuring at the selected bias points. This relatively small change should have a negligible impact on the resolution of the TES. The region in the superconducting transition where the bias points are selected is highlighted in figure 3.

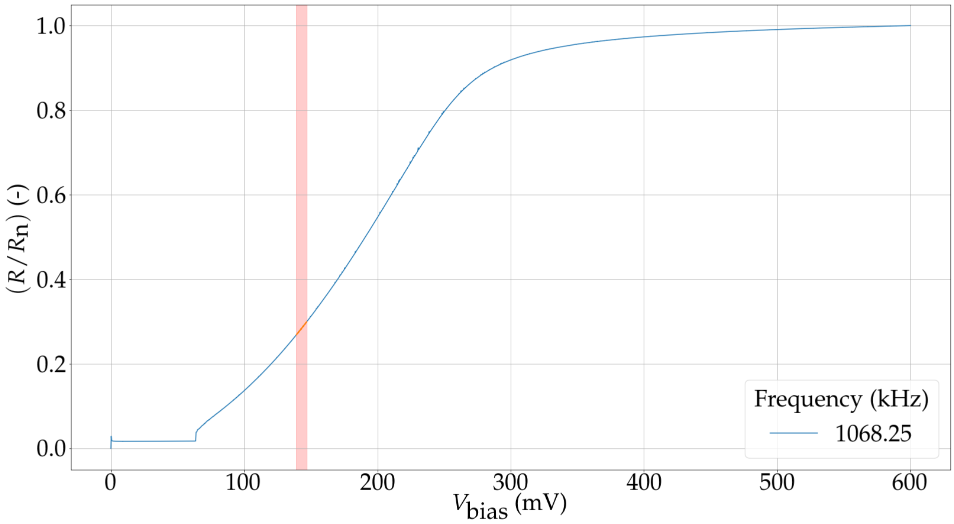

Figure 3: Normalized resistance R/R_n of the TES as a function of the AC-bias voltage $V_{\texttt{bias}}$. The region on the superconducting transition at which the measurement to determine the resolution dependency on the slope was done. In this region, the resistance of the TES is considered close to constant and changes no more than 4% compared to normal.

To acquire the value of the slope M in every bias point on the phase curve (figure 1), the derivative of this curve was calculated. Using this derivative, the slope at every bias point in the X-ray measurements was obtained. The measurement results of every point in this resolution vs slope measurement is given in table 1.

Table 1: Measurement results of the resolution ΔE as a function of the slope M at a given bias point.

M (deg/mV) $\pm$0.01 (deg/mV)	ΔE (eV)	δE (eV)
-0.31	2.43	0.15
-0.30	2.59	0.14
-0.28	2.56	0.13
-0.28	2.40	0.14
-0.26	2.61	0.14
-0.26	2.61	0.14
-0.23	2.18	0.15
-0.21	2.37	0.14
-0.18	2.63	0.15
-0.17	2.51	0.13
-0.14	2.57	0.15
-0.10	2.69	0.15
-0.10	2.72	0.13
-0.05	2.47	0.15
0.00	2.59	0.13
0.11	2.31	0.14
0.35	2.37	0.14
0.49	2.81	0.14
0.53	2.70	0.15
0.74	2.41	0.14
0.76	2.58	0.13

The resolution as a function of the slope has been plotted in figure 4. In this figure, more measurement points are present on a negative slope. This is because the oscillations in the phase are not symmetrical and have an inclination as is seen in figure 2.

A linear fit was made through the data which can be seen in figure 4. To determine if there is, in fact, any linear correlation in the data set, the pearson correlation [1] was calculated. From this calculation, a value of 0.15 was obtained, which indicates a positive, negligible correlation [2] between the two parameters.

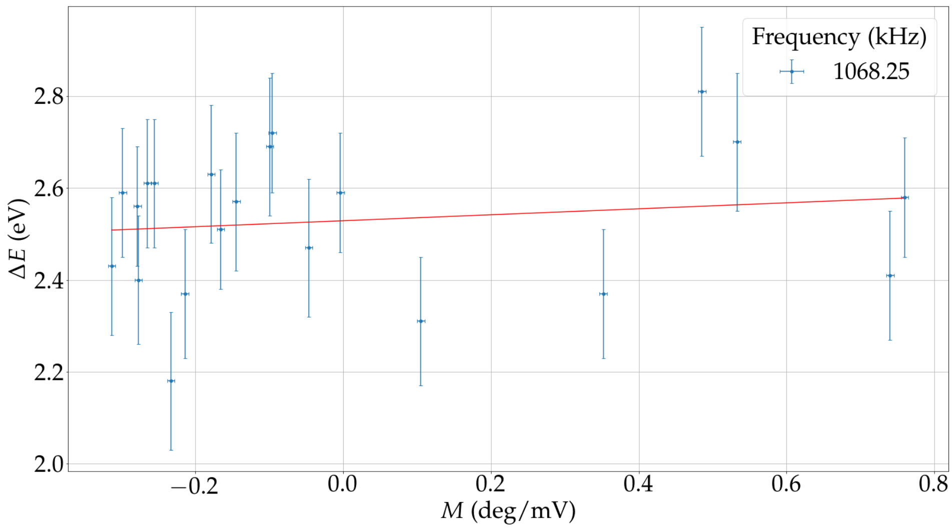

Figure 4: The energy resolution ΔE as a function of the slope M from the phase curve. In this figure, a linear fit is made through the data and is shown as a straight line. In the measured region, the resistance of the TES is considered close to constant.

3 Temperature Stability

It is important that the temperature is stable during measurements. For that reason, the temperature log is shown in figure 5. As can be seen, the temperature is stable at 60 mK with a scatter of 1 μK. This is sufficient enough for the measurements performed in this measurement report.

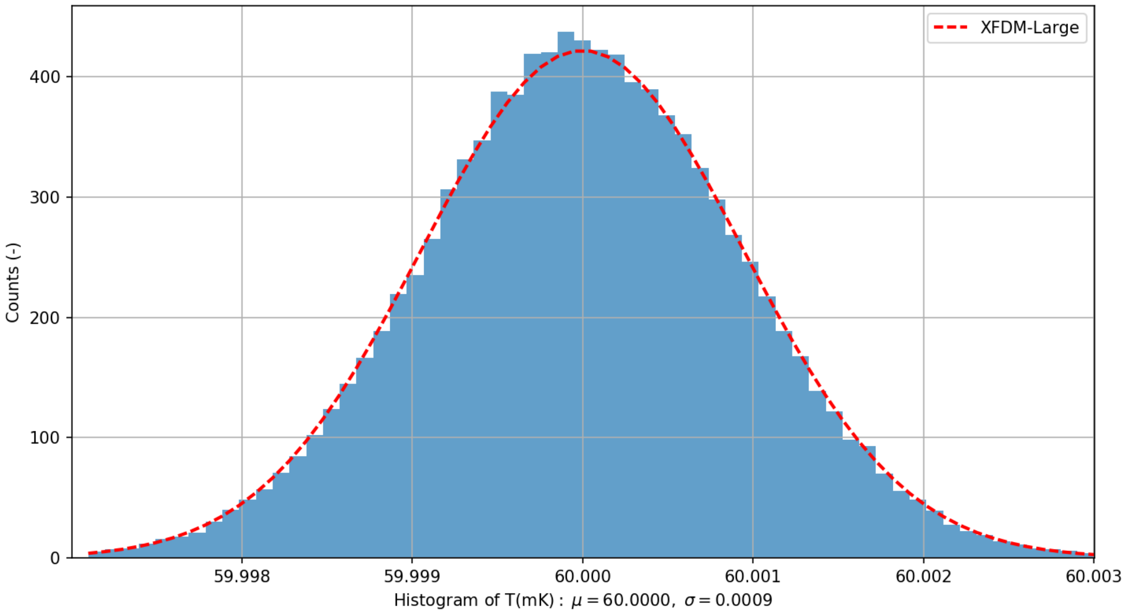

Figure 5: Temperature stability during the X-ray measurement of 5 April 2019. During this measurement, the temperature was stable at 60 mK with a scatter of 1 μK

4 Conclusion

The Pearson correlation coefficient between resolution and slope shows a value of 0.15. This concludes that there is a negligible correlation between the energy resolution and slope at a low-frequency AC-bias.

5 Discussion

It might be possible that while for low-frequency AC-bias the effect of the slope on the energy resolution is negligible, that for higher frequencies it is in fact important. For high frequencies, the weak link effect will cause a larger phase oscillation and Eddie currents to increase [3] at which choosing the right bias point could become of significant importance.

A similar measurement as the one in this report should be executed for a pixel that works at a higher frequency to check if any correlation exists between the slope at a bias point and the energy resolution.

References

[1] L. Statistics. Pearson product-moment correlation. [Online]. Available: https://statistics.laerd.com/statistical-guides/pearson-correlation-coefficient-statistical-guide.php

[2] P. AHAMMAD. (2016, nov) How to interpret correlation coefficients. [Online]. Available: http://www.parvez-ahammad.org/blog/how-to-interpret-correlation-coefficients

[3] K. Sakai, J. S. Adams, S. R. Bandler, J. A. Chervenak, A. M. Datesman, M. E. Eckart, F. M. Finkbeiner, R. L. Kelley, C. A. Kilbourne, A. R. Miniussi, F. S. Porter, J. S. Sadleir, S. J. Smith, N. A. Wakeham, E. J. Wassell, W. Yoon, H. Akamatsu, M. P. Bruijn, L. Gottardi, B. D. Jackson, J. van der Kuur, B. J. van Leeuwen, A. J. van der Linden, H. J. van Weers, and M. Kiviranta, "Study of Dissipative Losses in AC-Biased Mo/Au Bilayer Transition-Edge Sensors," *Journal of Low Temperature Physics*, vol. 193, pp. 356–364, Nov 2018.

Appendix 3

TES X-ray resolution dependency on AC-bias frequency and voltage

XFDM pixel 0, AC-bias frequency and voltage scan

Graduation project Applied Physics

Measurement Report

Executed By:
Gerwin Verkerk
BSc student at The Hague
University of Applied Sciences

Date: 03-22-2019
Department: Instrument Science

1 Measurement goal

The goal of this measurement is to characterize the response of a TES sensor to changes in AC-bias frequency and voltage. The energy resolution will be measured for different values of these two parameters and a correlation between them will be looked for. The measurement will be done using pixel 0 in the XFDM measurement setup.

2 Measurement results

2.1 Expected result

The TES-sensors of the XFDM measurement setup are made by NASA Goddard and are expected to give an energy resolution of below 2.5 eV when tuned correctly. This is therefore also the expected resolution that will be obtained from the measurements.

The TES sensors are connected to LC-circuits. Each of these circuits has a specific resonance frequency to which the AC-bias frequency has to match. When the frequency matches closely to this resonance frequency, the signal to noise ratio (SNR) of the TES will be high. When this is the case, the energy resolution should be high.

The bias voltage determines the part of the superconducting transition at which a measurement is done. When an X-ray photon hits the detector, the temperature of the TES will change which is shown as a shift in the superconducting transition. If the bias point is chosen low in transition, the detector will stay in the superconducting transition when the photon hits and give the biggest response. This should give a high energy resolution.

2.2 Results

The energy resolution of the TES has been measured at a specific range of frequencies going from 1068,24 kHz to 1068.35 kHz with a step size of 0.01 kHz. For each of these frequencies, 4 different bias points have been selected at 110 mV, 120 mV, 130 mV and 140 mV. For each of these points, an X-ray resolution measurement of 3000 counts was done. Besides resolution measurements, IV-curves were made for each of the frequencies in range.

The measured IV-curves are shown in figure 1. The bias points for each of the curves at which an X-ray resolution measurement was done are indicated by a red X.

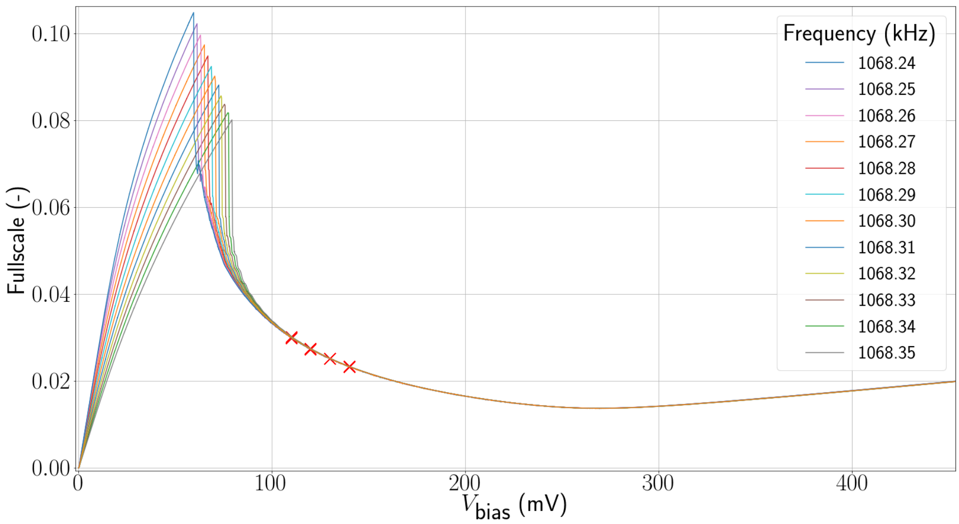

Figure 1: IV-curve measurements for frequencies going from 1068.24 kHz up to 1068.35 kHz with a step size of 0.01 kHz. The selected bias point are indicated by an red X for each of the frequencies.

The results of the energy resolution ΔE measurements at specific bias frequency f and bias V_{bias} voltage are displayed in table 1. The statistical uncertainty of the energy resolution δE is calculated using the Poisson distribution.

Table 1: Measurement data of X-ray energy resolution ΔE as a function of AC-bias frequency f and voltage V_{bias}. One sigma σ error in resolution is given by δE

f (kHz) $\pm$0.005 kHz	V_{bias} (mV) $\pm$0.01 mV	ΔE (eV)	δE (eV)
1068.24	110.12	2.14	0.23
1068.24	119.89	2.63	0.22
1068.24	129.95	2.74	0.19
1068.24	140.02	2.91	0.20
1068.25	110.12	2.50	0.23
1068.25	119.89	2.49	0.21
1068.25	129.95	2.69	0.21
1068.25	140.02	2.02	0.21
1068.26	110.12	2.72	0.21
1068.26	119.89	2.40	0.22
1068.26	129.95	2.35	0.21
1068.26	140.02	2.45	0.20
1068.27	110.12	2.34	0.21
1068.27	119.89	2.14	0.22
1068.27	129.95	2.67	0.20
1068.27	140.02	2.29	0.21
1068.28	110.12	2.71	0.22
1068.28	119.89	2.46	0.21
1068.28	129.95	2.76	0.21
1068.28	140.02	2.33	0.23
1068.29	110.12	2.57	0.22
1068.29	119.89	2.62	0.19
1068.29	140.02	2.40	0.20
1068.30	110.12	2.58	0.21
1068.30	119.89	2.56	0.22
1068.30	129.95	2.44	0.21
1068.30	140.02	2.58	0.20
1068.31	110.12	2.79	0.21
1068.31	119.89	2.56	0.20
1068.31	129.95	2.64	0.21
1068.31	140.02	2.83	0.23
1068.32	110.12	2.38	0.22
1068.32	119.89	2.52	0.23
1068.32	129.95	2.45	0.20
1068.32	140.02	2.39	0.21
1068.33	110.12	2.69	0.24
1068.33	119.89	2.51	0.22
1068.33	129.95	2.83	0.22
1068.33	140.02	2.70	0.22
1068.34	110.12	4.87	0.23
1068.34	119.89	2.66	0.22
1068.34	129.95	2.62	0.21
1068.34	140.02	2.27	0.21
1068.35	119.89	3.87	0.25
1068.35	129.95	2.67	0.23
1068.35	140.02	2.44	0.20

2.3 Analysed results

A plot with the energy resolution as a function of bias frequency and voltage has been made and is shown in figure 2. A lower value for the resolution ΔE means a higher distinctiveness between energies and a better energy resolution.

Due to the relatively low amount of counts, the inaccuracy of the measurements is quite high. One sigma error is already around 0.2 eV as can be seen in table 1. This means a lot of values overlap and the graph should be looked at with caution.

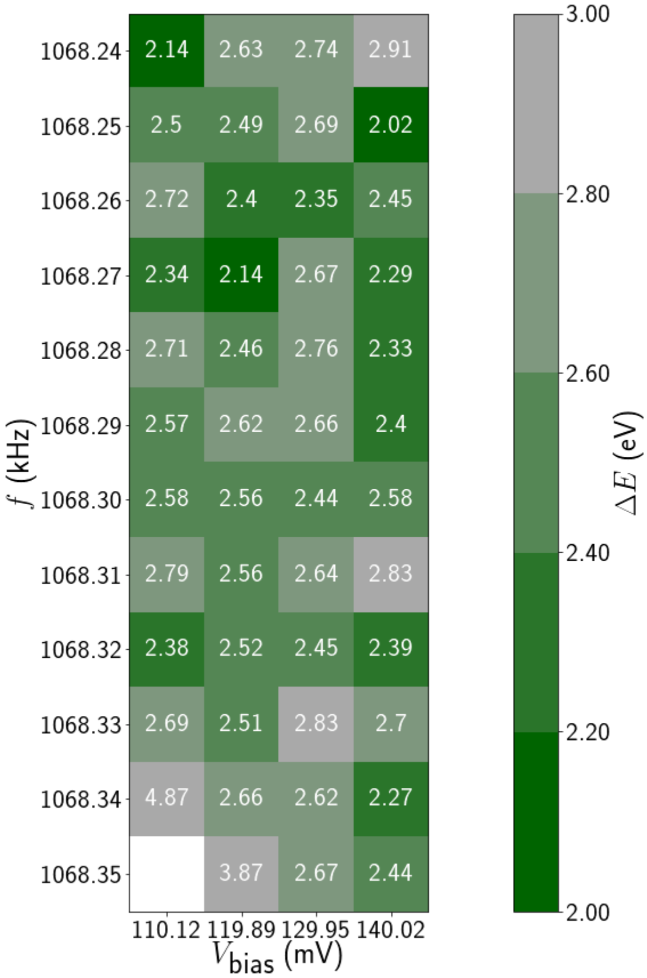

Figure 2: TES energy resolution as a function of the bias frequency f and voltage V_{bias}. This plot was made using pixel 0 in the XFDM setup.

From the plot, no direct conclusions can be made relating to the energy resolution its dependency on the bias frequency and voltage. The scanned range of frequencies and voltages is too small to see any of big change. Besides that, the frequency influences the resistance of the LC-circuit, which has not been taken into account during this measurement.

However, what can be seen is that the energy resolution, even outside three sigma error, changes when the bias frequency and voltage changes. Whether this is can be directly linked to frequency and voltage dependency cannot be said from the obtained result. It could be possible that one or more other parameters besides bias frequency and voltage were changed without intention. Further investigation would be needed to draw any of direct conclusions.

2.4 Temperature variation

To achieve a good measurement result, it is important for the temperature of the TES to be stable around 60 mK. The temperature scatter has been monitored during the measurement and is shown in figure 3. During the measurement, the scattering is no more than 1 µK at one σ error.

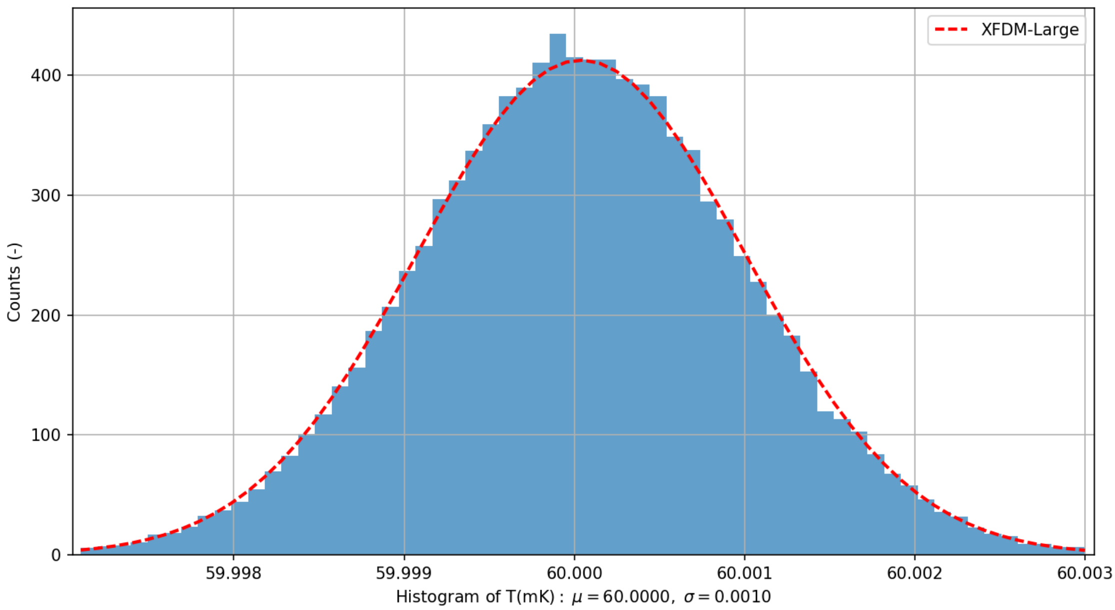

Figure 3: Temperature scatter over the course of the measurement on the 22nd of March 2019. As can be seen from the plot, during the measurement, the temperature was stable at 1 µK for one σ error.

3 Conclusion

No direct conclusions can be made regarding the dependency of the energy resolution on bias frequency and voltage. However, outside of the error margins, there is a significant enough change that some dependency could be present. To make any conclusions for the case this is true, further investigation is needed.

4 Discussion

The changes in energy resolution when the bias frequency and voltage are changed could mean there is a dependency between the parameters. However, it cannot be said with certainty that no other parameters were unintentionally changed in the background. To make any conclusions on this matter, the system could be checked for consistency in the given result.

Appendix 4

Netherlands Institute for Space Research

TES X-ray resolution dependency on AC-bias frequency and voltage

XFDM pixel 0, AC-bias frequency and electrical transfer function scan. Dual-FEE electronics

Graduation project Applied Physics

Measurement Report

Executed By:
Gerwin Verkerk
BSc student at The Hague
University of Applied Sciences

Date: 03-22-2019
Department: Instrument Science

1 Measurement goal

The goal of this measurement is to find a correlation between X-ray energy resolution and any of TES properties. In this report, a correlation between the AC-bias frequency and the X-ray energy resolution is searched for. Besides that, a dependency between the electrical transfer function of the feedback circuit and the energy resolution is investigated. For this measurement, pixel 0 in the XFDM setup of SRON is used.

2 Measurement results

To search for a relationship between AC-bias frequency and the energy resolution, a long measurement of 6000 counts measurement point was taken. This was done for two bias voltages of 110 mV and 130 mV. For each of these bias voltages, a frequency scan ranging from 1068.0 kHz up to 1068.5 kHz was done. The motivation in choosing this frequency range is that it covers the part of the ABC-circuit resonance frequency and the FB-circuit resonance frequency peaks.

2.1 Expected result

When the AC-bias frequency is equal to the resonance frequency of the LC-circuit, all signal is expected to pass through. At this frequency, the energy resolution of the TES would, therefore, be expected to high.

However, when the circuit is operational, a feedback-line is connected. This feedback line induces a parasitic inductance and has its own resonance frequency. The resonant frequency of this circuit is kept close to that of the LC-circuit in the AC-bias line but a small shift is present.

If the energy resolution is sensitive to this small change in resonance frequency for the tuning of the AC-bias frequency, then the optimal point would be expected to lay in between these two resonances.

2.2 Results

Below the results of the network analyser scan and resolution dependency on AC-bias frequency are presented.

2.2.1 Network Analyser Scan

For the AC-bias line, a sharp peak can be found around the resonance frequency of the LC-filter in question. This peak lays around 1068.26 kHz for pixel 0. For the FB-line, it is different. It also has a peak around 1068.26 kHz due to the FB-line 'seeing' the LC-circuit in the AC-bias line. But it also has a trough which is caused by a slight difference in common inductance between the input and output coil.

The NWA scan for the AC-bias line can be seen in figure 1.

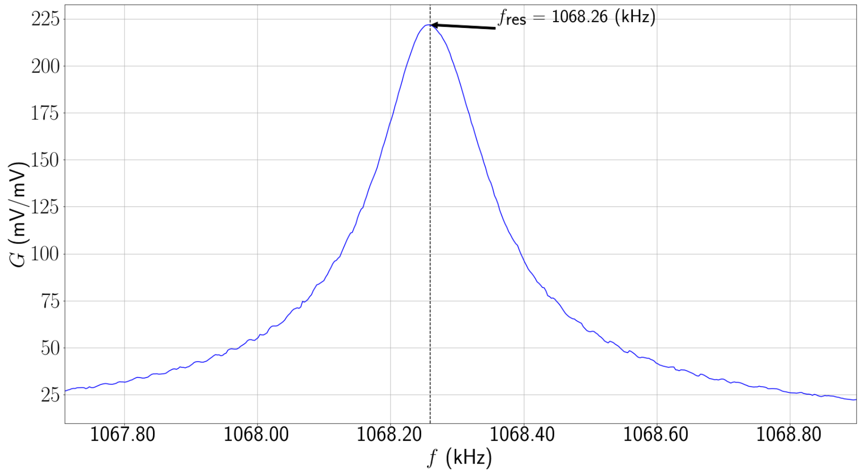

Figure 1: Network analyser scan for the AC-bias line. In this figure, the resonance frequency of the LC-filter can be seen around 1068.26 kHz.

The NWA scan for the FB-bias line can be seen in figure 2.

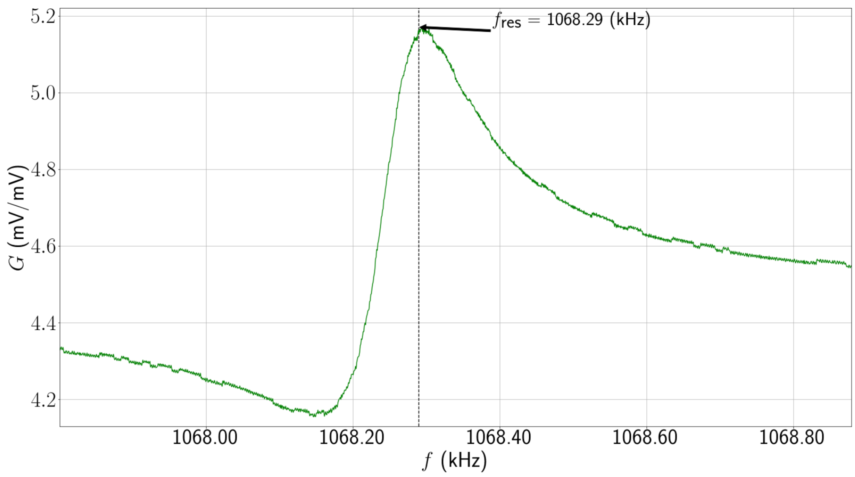

Figure 2: Network analyser scan for the FB-Bias line. The feedback circuit 'sees' the electrical circuit of the AC-Bias line and therefore a frequency is present close to equal to that of the LC-filter resonance frequency. The dip is caused by the difference between the input and output coil in the electrical circuit which induces a parasitic inductance.

2.2.2 Resolution dependency on AC-bias frequency

The measurement results for the X-ray energy resolution as a function of AC-bias frequency is given in tables 1 and 2. These two bias voltages were chosen because they gave a good energy resolution in a past measurement.

Table 1: Measurement results of X-ray energy resolution as a function of AC-bias frequency. For every bias point, the AC-bias voltage was kept constant at 130 mV. 6000 counts per bias point were set.

f **(kHz)** $\pm$**0.005 kHz**	ΔE **(eV)**	δE **(eV)**
1068.02	3.60	0.14
1068.05	2.58	0.14
1068.08	2.69	0.14
1068.10	2.79	0.15
1068.13	2.96	0.14
1068.15	2.77	0.15
1068.18	2.51	0.15
1068.20	2.64	0.13
1068.22	2.66	0.14
1068.25	2.63	0.15
1068.27	2.57	0.15
1068.30	2.42	0.14
1068.33	2.58	0.14
1068.35	2.49	0.14
1068.38	2.47	0.15
1068.40	2.47	0.14
1068.43	2.71	0.14
1068.45	2.66	0.14

Table 2: Measurement results of X-ray energy resolution as a function of AC-bias frequency. For every bias point, the AC-bias voltage was kept constant at 110 mV. 6000 counts per bias point were set.

f **(kHz)** $\pm$**0.005 kHz**	ΔE **(eV)**	δE **(eV)**
1068.05	3.53	0.15
1068.13	2.81	0.14
1068.15	2.48	0.14
1068.18	2.76	0.15
1068.20	2.59	0.13
1068.22	2.72	0.14
1068.25	2.89	0.15
1068.27	2.26	0.14
1068.30	2.37	0.14
1068.33	2.64	0.14
1068.35	2.68	0.15
1068.38	2.99	0.14
1068.40	2.96	0.16
1068.43	3.47	0.14
1068.45	3.96	0.15

The measurement data has been plotted and is shown in figure 3. In this figure, the X-ray energy resolution as a function of the AC-bias frequency is presented. Besides that, the electrical transfer function G of the FB-line is plotted as a function of the AC-bias frequency.

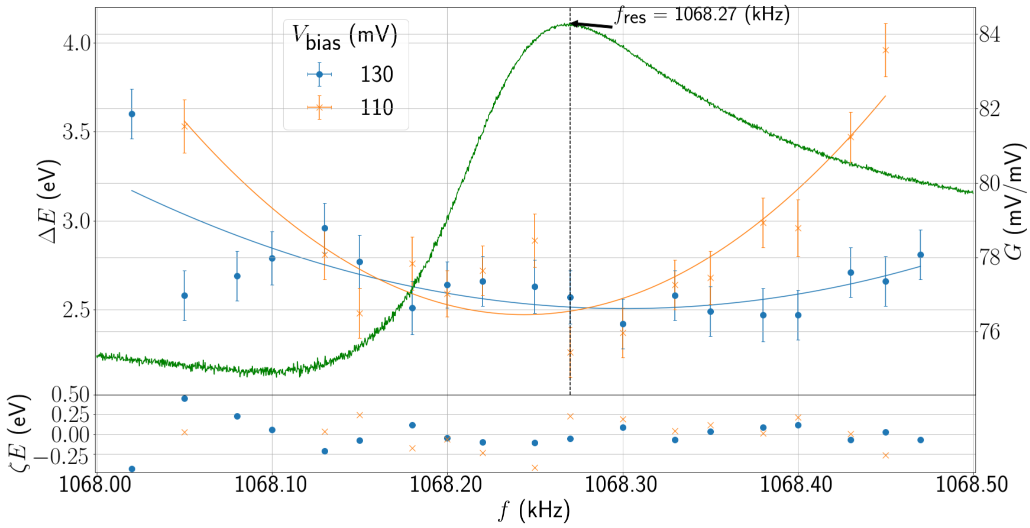

Figure 3: X-ray energy resolution as a function of the AC-bias frequency. In this plot, a 2nd order polynomial fit was made through the data points to see if any clear correlation between these parameters is present. The electrical transfer function of the FB-circuit is also plotted on top to give an overview of how the energy resolution is distributed along with the resonance frequency.

The fit that has been put through the data is a standard second order polynomial. This polynomial was chosen as a way to describe the observed data distribution and was not derived from theory. When looking at the fit with a biased eye, one could claim that a second order polynomial correlation is present between the data points. To test if this is correct, the weighted chi-square test for goodness of fit was calculated. The value that came out of this calculation was 29.29 for the blue line and 25.37 for the orange one. The blue data points have 16 DoF (Degrees of Freedom) and the orange ones have 12 DoF. According to [1][2], these calculated values for chi-squared give a possibility that these fits are correct of less than 0.5% for the blue line and less than 10% for the orange one. It can, therefore, be said with said certainty, that for the given data sets, the distribution does not follow any kind of second order polynomial.

When looking at the data with the eye, it can be seen that close to the resonance frequency of the LC-resonator the X-ray energy resolution is good for both the 130 mV and 110 mV points. There seems to be an important dependency which can not be determined given the obtained data set. More measurements at the same bias points should be taken and from those, an average can be determined which could show the dependency that is present.

2.3 Temperature variation

In order to obtain good measurement results, it is important for the temperature of the setup to be stable. For this reason, the temperature is logged for every measurement. The temperature scatter during the measurement discussed in the report is shown in the sections below. The measurement discussed in this measurement report made use of the Dual-FEE electronics. This measurement started on the 18th of April and ended on the 21st of April. In the sections below, the temperature scatter during the course of the measurement is given.

2.3.1 Temperature scatter 18th of April

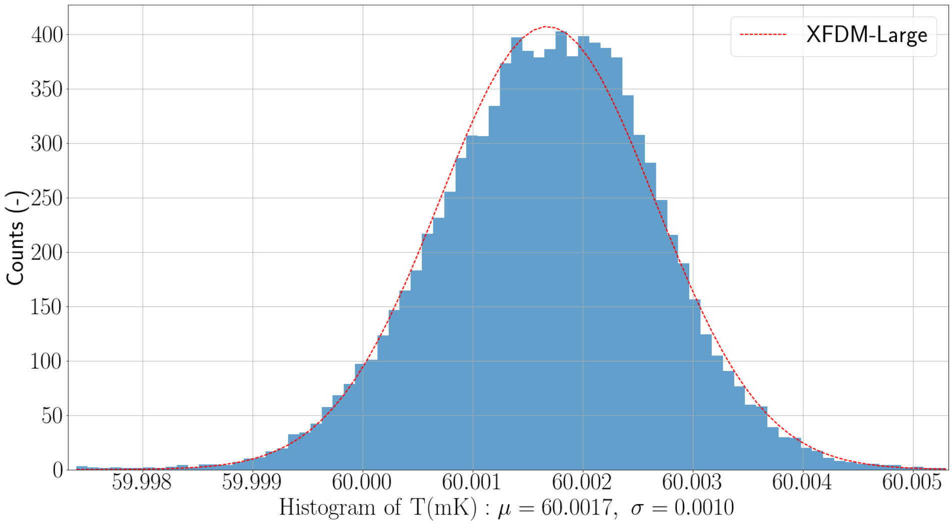

Figure 4: Temperature scatter over the course of the measurement on the 18th of April 2019. As can be seen from the plot, during the measurement, the temperature was stable at 1 μK for one σ error.

2.3.2 Temperature scatter 19th of April

The file in which the temperature scatter of the 19th of April was logged has gotten corrupt. For this reason, the temperature stability for this day is uncertain. However, there is no reason to suspect that it has varied significantly during the measurements. But it should be kept in mind.

2.3.3 Temperature scatter 20th of April

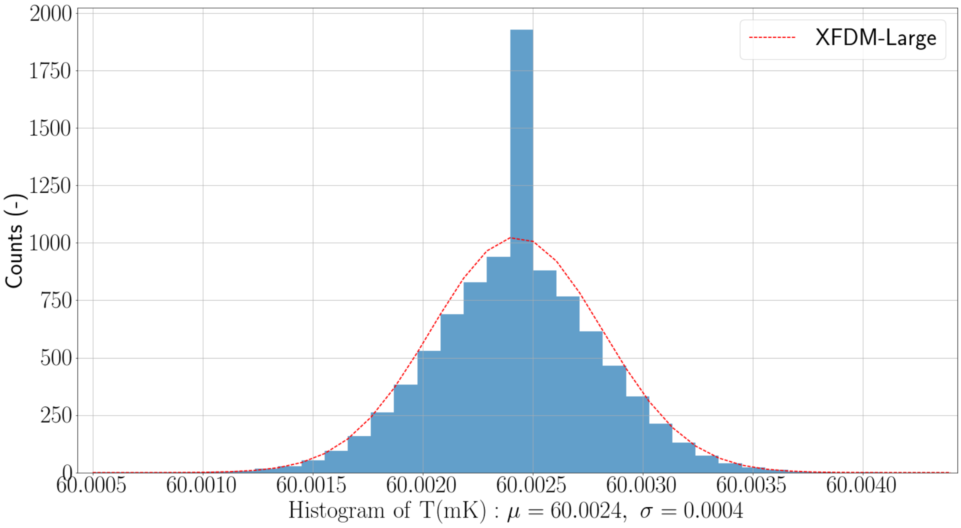

Figure 5: Temperature scatter over the course of the measurement on the 20th of April 2019. As can be seen from the plot, during the measurement, the temperature was stable at 0.4 μK for one σ error.

2.3.4 Temperature scatter 21st of April

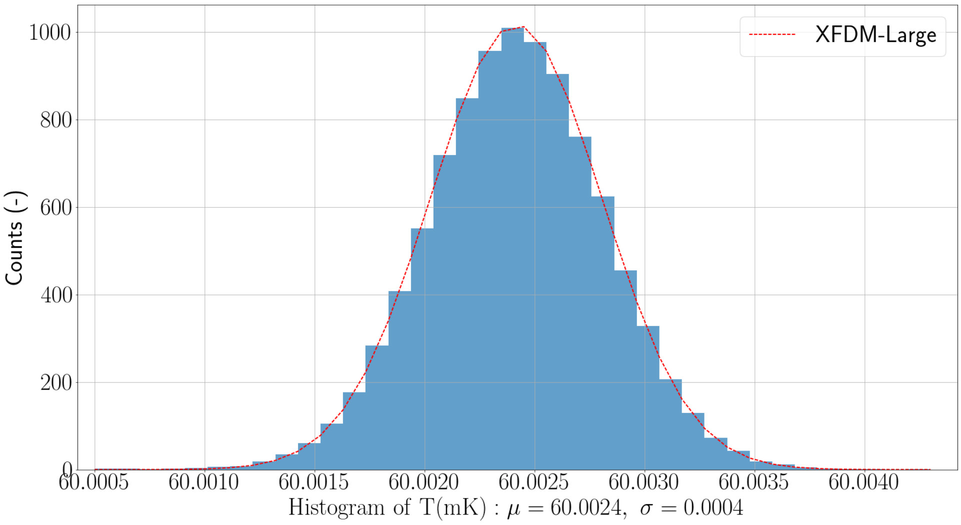

Figure 6: Temperature scatter over the course of the measurement on the 21st of April 2019. As can be seen from the plot, during the measurement, the temperature was stable at 0.4 μK for one σ error.

3 Conclusion

The dependency between the X-ray energy resolution and AC-bias frequency does not follow any kind of second-order polynomial as has been verified from the chi-square test for goodness of fit.

4 Discussion

Although a second-order polynomial is unable to describe the correlation between the X-ray energy resolution and frequency it does not mean the parameters are not connected to each other. It is well known that if the bias-frequency is too far off that of the resonance frequency of the LC-resonator, the resolution will get worse. This can also be seen in the obtained measurement result. However, the spread in the data is too large to conclude anything regarding the optimum frequency between the LC-resonator resonance frequency and the trough in the FB-line. To reduce the spread, an average of multiple measurements, at the same bias points, can be taken. Another possibility is to take the measurement for a pixel that is biased with a higher frequency since the distance between the resonance peak and trough is dependent on frequency.

References

[1] Hinkle, Wiersma, and Jurs. Chi-square test for goodness of fit. [Online]. Available: http://www.phy.ilstu.edu/slh/chi-square.pdf

[2] medcalc. Values of the chi-squared distribution. [Online]. Available: https://www.medcalc.org/manual/chi-square-table.php

Appendix 5

Single-FEE measurement results

In the tables 1 and 2 below, the measurement result for the X-ray resolution dependency on the AC-bias frequency is given. For both tables, two bias voltages were picked which were kept constant over the measured frequency range.

Table 1: Measurement results of X-ray energy resolution dependency on AC-bias frequency. Measurement was taken for two bias points at 110 mV and 130 mV. The Dual-FEE electronics were used during this measurement.

f **(kHz)** $\pm$**0.005 kHz**	$V_{\mathbf{bias}}$ **(mV)** $\pm$**0.01 mV**	ΔE **(eV)**	δE **(eV)**
1068.02	110.12	15.48	0.61
1068.02	129.95	3.60	0.14
1068.05	110.12	3.53	0.15
1068.05	129.95	2.58	0.14
1068.08	110.12	4.12	0.16
1068.08	129.95	2.69	0.14
1068.10	110.12	4.68	0.14
1068.10	129.95	2.79	0.15
1068.13	110.12	2.81	0.14
1068.13	129.95	2.96	0.14
1068.15	110.12	2.48	0.14
1068.15	129.95	2.77	0.15
1068.18	110.12	2.76	0.15
1068.18	129.95	2.51	0.15
1068.20	110.12	2.59	0.13
1068.20	129.95	2.64	0.13
1068.22	110.12	2.72	0.14
1068.22	129.95	2.66	0.14
1068.25	110.12	2.89	0.15
1068.25	129.95	2.63	0.15
1068.27	110.12	2.26	0.14
1068.27	129.95	2.57	0.15
1068.30	110.12	2.37	0.14
1068.30	129.95	2.42	0.14
1068.33	110.12	2.64	0.14
1068.33	129.95	2.58	0.14
1068.35	110.12	2.68	0.15
1068.35	129.95	2.49	0.14
1068.38	110.12	2.99	0.14
1068.38	129.95	2.47	0.15
1068.40	110.12	2.96	0.16
1068.40	129.95	2.47	0.14
1068.43	110.12	3.47	0.14
1068.43	129.95	2.71	0.14
1068.45	110.12	3.96	0.15
1068.45	129.95	2.66	0.14
1068.47	110.12	4.24	0.14
1068.47	129.95	2.81	0.14

Table 2: Measurement results of X-ray energy resolution dependency on AC-bias frequency. Measurement was taken for two bias points at 120 mV and 140 mV. The Single-FEE electronics were used during this measurement.

f (kHz) $\pm$0.005 kHz	V_{bias} (mV) $\pm$0.01 mV	ΔE (eV)	δE (eV)
1068.00	119.89	3.94	0.13
1068.00	140.02	3.44	0.12
1068.02	140.02	3.47	0.12
1068.05	119.89	3.55	0.11
1068.05	140.02	2.72	0.11
1068.08	119.89	3.14	0.12
1068.08	140.02	2.85	0.13
1068.10	119.89	2.90	0.12
1068.10	140.02	3.08	0.13
1068.13	119.89	3.10	0.12
1068.13	140.02	2.88	0.12
1068.15	140.02	2.83	0.12
1068.18	119.89	3.88	0.13
1068.20	119.89	2.93	0.12
1068.20	140.02	2.90	0.12
1068.22	119.89	2.98	0.12
1068.22	140.02	2.68	0.12
1068.25	119.89	2.77	0.13
1068.25	140.02	2.68	0.13
1068.27	119.89	2.81	0.13
1068.27	140.02	2.61	0.11
1068.30	119.89	2.67	0.12
1068.30	140.02	2.79	0.12
1068.33	119.89	2.71	0.11
1068.33	140.02	2.81	0.12
1068.35	119.89	2.95	0.12
1068.35	140.02	2.53	0.12
1068.38	119.89	2.54	0.12
1068.38	140.02	2.78	0.12
1068.40	119.89	2.85	0.12
1068.40	140.02	2.66	0.13
1068.43	119.89	2.86	0.12
1068.43	140.02	2.67	0.12
1068.45	119.89	3.17	0.12
1068.45	140.02	2.75	0.12
1068.47	119.89	3.47	0.13
1068.47	140.02	3.00	0.12
1068.50	119.89	3.46	0.13
1068.50	140.02	2.86	0.13